

**Alma Mater Studiorum – Università di bologna**

---

SCUOLA DI SCIENZE

Dipartimento di Chimica Industriale “Toso Montanari”

Corso di Laurea Magistrale in

**Chimica Industriale**

Classe LM-71 - Scienze e Tecnologie della Chimica Industriale

**Atropisomeric 1,2-dibenzoazaborines:  
Synthesis and Dynamic Studies.**

Tesi di laurea sperimentale

**CANDIDATO**

Maria Boffa

**RELATORE**

**Prof. Dr** Andrea Mazzanti

**CORRELATORE**

**Dr** Michele Mancinelli

**Sessione I**

---

**Anno Accademico 2017-2018**

---



## ABSTRACT

In this thesis project we have studied new atropisomeric molecules that have a nitrogen-boron bond in an aromatic cyclic system, namely the 1,2-dibenzoazaborine structure. We have synthesized molecules that have a stereogenic boron-aryl axis with different steric hindrance in the *ortho* position of the aryl ring (compounds **5**). The synthesis reaction was optimized for compound **5a** and then we introduced a chirality probe to follow the dynamic process by NMR (e.g. an ethyl group in product **5b** and an isopropyl group in the product **5c**). We have analyzed the molecules with NMR spectroscopy at variable temperature (VT), dynamic HPLC and kinetics studies to determinate the racemization energy barrier. Where possible (compound **5d**), we have assigned the absolute configuration of the atropisomers by ECD (Electronic Circular Dichroism) methods and by TD-DFT (Time Dependent – Density Functional Theory) calculation.

## SOMMARIO

Questo progetto di tesi è stato indirizzato verso lo studio di nuove molecole atropisomeriche contenenti un legame azoto-boro all'interno di un sistema ciclico aromatico, in particolare è stata presa in esame la struttura della dibenzoazaborina. Sono state sintetizzate molecole che presentano un asse di chiralità boro-arile e con differente ingombro sterico in *orto* all'arile (composto **5**). La sintesi è stata prima messa a punto sull'*orto*-tolile (**5a**) e in seguito è stato introdotto un probe di chiralità per lo studio dinamico NMR (etile nel prodotto **5b**, isopropile nel prodotto **5c**). Le molecole ottenute sono state analizzate attraverso analisi NMR a temperatura variabile (VT), dinamica HPLC e studi cinetici per determinare l'energia della barriera rotazionale. In fine, è stata assegnata la configurazione assoluta dei due atropisomeri del composto **5d** mediante il metodo ECD (Dicroismo Circolare Elettronico) e calcoli di tipo TD-DFT (Teoria del Funzionale di Densità Dipendente dal Tempo).



# Index

<b>1</b>	<b>Introduction</b>	<b>1</b>
1.2	Azaborines	1
1.3	Chirality	3
1.4	Atropisomer	4
<b>2</b>	<b>Aim of thesis</b>	<b>8</b>
<b>3</b>	<b>Results and discussion</b>	<b>10</b>
3.1	Synthesis of the 2,4,6-triphenylaniline <b>1</b>	11
3.2	Optimization of synthesis of 1,2-dibenzoazaborine <b>5</b>	13
3.3	Attempts of synthesis of 1,2-dibenzoazaborinine <b>8</b>	15
3.4	Synthesis of 1,2-dibenzoazaborine <b>5b</b>	16
3.5	Conformational studies of 1,2-dibenzoazaborine <b>5b</b>	16
3.6	Synthesis of 1,2-dibenzoazaborinine <b>5c</b>	22
3.7	Conformational and kinetic studies of 1,2-dibenzoazaborine <b>5c</b>	22
3.8	Synthesis of 1,2-dibenzoazaborinine <b>5d</b>	30
3.9	Conformational studies of 1,2-azaborines <b>5d</b>	30
<b>4</b>	<b>Absolute configuration of compound <b>5d</b></b>	<b>37</b>
<b>5</b>	<b>Conclusion</b>	<b>41</b>

<b>6 Experimental section</b>	<b>43</b>
6.1 Materials	43
6.2 Instruments	43
6.3 Computational calculations	44
6.4 Synthesis and Characterization	44
6.4.1 2,4,6-triphenylaniline (1)	44
6.4.2 Aryl Grignard preparation (4)	45
6.4.3 General procedure for the preparation of 1,2-dibenzoazaborine (5)	45
6.4.4 1-bromo-2-isopropoxynaphthalene (9)	48
<b>7 Appendix</b>	<b>50</b>
7.1 Density Functional Theory DFT	50
7.2 Dynamic stereochemistry analysis and methodologies	52
7.2.1 Dynamic Nuclear Magnetic Resonance D-NMR	52
7.2.2 Dynamic High Pressure Liquid Chromatography D-HPLC	54
7.3 Time Depend- Density Functional Theory TD-DFT	55
7.4 Electronic Circular Dichroism ECD	55
<b>8 Reference</b>	<b>58</b>

# 1.Introduction

## 1.1 Azaborines

Azaborines (**II**) are part of a class of chemical compounds that is affecting a large part of researchers, especially in recent years. The azaborine structure replaces a C=C bond with an N-B bond within any molecular structure change, to obtain isosteric and isoelectronic architectures. The isosteric and isoelectronic terms mean respectively: molecules or fragments of molecules that contain the same number of atoms and the same arrangement of electrons. The most important compounds that contain the boron-nitrogen bond are cyclic, isoelectronic to benzene (**I** and **II** in Figure 1).

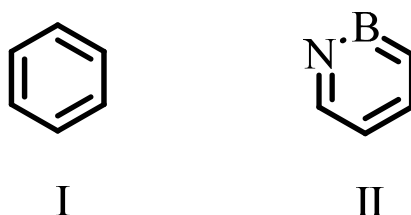


Figure 1. **I** benzene, **II** azaborine.

The polarity of the B-N bond imparts different chemical and physical properties to the molecular structure. Since boron and nitrogen have very different electronegativity,  $\pi$  electrons are mainly positioned around nitrogen, which means that the structure is slightly less aromatic and less stable. Since these two atoms have different polarities we have the formation of a local dipole moment which significantly alter both the optical properties and the structure of the solid state. This happens because it changes the character of the boundary molecular orbitals and the intermolecular interactions present in the solid state. Depending on the position of the two atoms in the ring three isomers are possible: 1,2-azaborine (**II**), 1,3-azaborine (**III**), 1,4-azaborine (**IV**) (Figure 2).

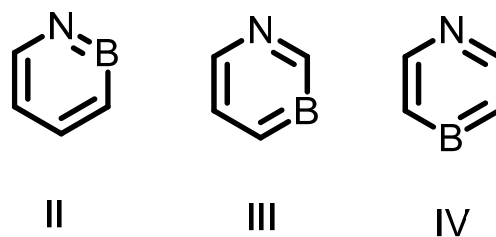


Figure 2. Different types of azaborine.

Among these, 1,2-azaborine are the most studied because they are easily accessible and stable. In these structures the nitrogen atom formally holds a positive charge and the boron a negative charge. X-ray studies and computational studies show a planar structure for all three isomers, thus demonstrating the presence of aromatic character and electronic delocalization, just as happens in the case of benzene (**I**). Compared to the same isosteric and isoelectric compounds, the length of C=C bond is shorter than B-N bond, 1.38 Å and 1.43 Å respectively. The inclusion of heteroatoms and  $\pi$ -conjugated fragments is a strategy that allows to find new materials with unique functions because the presence of this link can change the electronic and photophysical properties of potential organic semiconductors. Replacing one or more of the carbon atoms in polycyclic aromatic hydrocarbons (PAHs) with boron decreases the HOMO-LUMO gap material providing access to molecule with chemiluminescent properties. Azaborines have been shown to function as organic light-emitting diodes (OLEDs)<sup>1</sup> and organic field-effect transistors (OFETs).<sup>2</sup> In addition to this, these types of organic compounds are important for the research of additional structures with biological functions for the research of new drugs. The latter concept is very interesting because the trivalent structure of the boron can give an alternative electrostatic contact with the enzymatic targets.

Azaborines are also used in the study of the rotation barrier of atropisomeric compounds with boron-aryl axis.<sup>3</sup> The length of boron-aryl axis is 1.58 Å, longer than the Csp<sup>2</sup>-aryl bond (1.49 Å). Moreover, the length of the bond is due to the fact that the aryl group is positioned perpendicular to the rest of the structure so, it cannot develop conjugation with the 1,2-dibenzoazaborine ring. This notion is important to understand the smaller rotational energy barrier in these types of compound. In fact, the two parts of the molecule being further away make easier the rotation around the chiral axis.

## 1.2 Chirality

The existence of molecules that have the same atomic connectivity but differ in the spatial arrangement of atoms, determines the existence of the concept of conformational isomerism. Chirality is a type of conformational isomerism that makes two objects, or two molecules as in our case, mirror images and therefore not superimposable to one another. The word chirality derives from the Greek, “**χειρ (kheir)**”, which means "hand", a familiar chiral object.<sup>4</sup> In 1848, the compresence and significance of chirality was recognized by Louis Pasteur, one of the pioneering of the stereochemistry, which prompted his famous statement of chiral universe (*l'univers est dissymetrique*).<sup>5</sup> Chiral objects defined in this way are called enantiomers. Chiral molecules are interesting because they have the same chemical and physical properties, but they can, for example, completely interact differently with biological molecules such as DNA, carbohydrates and chiral proteins. In the literature, especially in the pharmaceutical field, many examples of chiral molecules are reported which give a positive or negative effect depending on the enantiomer that is reacted. A well renowned example of a chiral drug is thalidomide that undergoes enantioconversion under physiological conditions. In the fifties and sixties, this drug was prescribed to pregnant women to alleviate morning sickness and it was sold in racemic form. The problem was that one of enantiomeric forms of thalidomide has sedative and antinausea effects, but the other enantiomer is a potent teratogen for the fetus.<sup>6</sup> This concept has paved the way for an increasingly in-depth research into methods of asymmetric synthesis<sup>7</sup> and analysis of enantiomerically pure molecules.

Chirality in a molecule can be given by several factors. The most common type of chirality is that described by an atom of carbon defined chiral centre of the molecule, which has four different substituents, then the same atomic connectivity, oriented differently in space. The two examples are therefore mirror-like and therefore called enantiomers. Another way of obtaining two chiral molecules is the presence of a chiral axis. For example, the 180° rotation of an asymmetric aryl around a bond holding the rest of the structure still, leads to a different conformation with respect to the initial one.

These two conformations are mirror images of each other and they cannot be superimposed. This type of conformational isomerism is called atropisomerism.

## 1.2 Atropisomers

The term atropisomer was coined for the first time by Khun in 1933,<sup>7</sup> it derives from the Greek "a" + "tropos" which means precisely "without movement". In order to have atropisomers the rotation around a single bond should be frozen due to the steric hindrance between the two groups bonded to give a chiral axis. In fact, this type of isomerism is due to the global symmetry of the molecule. The first definition does not give any definition about the stability of the atropisomers and about the rotational energy barrier of the stereogenic axis. For this reason, Oki<sup>8</sup> improved the definition of atropisomers. He suggested that an atropisomer is a conformer that interconverts quite slowly (rotation barrier 21.8 kcal·mol<sup>-1</sup> at +25 °C) upon bond rotations which has a half-life of at least 1000 s (at +25 °C) so you can separate the enantiomers physically. Today, this notion is still not exhaustively defined, in the last years; LaPlante proposed a map of stereogenic axes stability (Figure 3).<sup>9</sup> They said that atropisomers can be divided into three classes based on values of rotational energy barriers.

- 1. Class 1:** Molecules that have a fast axial rotation rates, to the order of nanoseconds to few seconds. So, at room temperature they are not observable and therefore, they can be considered as single entities. In this case the energy barrier has values less than 19 kcal·mol<sup>-1</sup>.
- 2. Class 2:** Molecules that are in a metastable situation and the values of the rotational energy barrier is between 20 and 30 kcal·mol<sup>-1</sup>. The half-life time ( $t_{1/2}$ ) range is from a few minutes to years. At room temperature some of this type of molecule cannot be physically separated but they show some features that make possible their definition of atropisomeric compounds. This class can be further divided into 2 subclasses:
  - 2.1. Class 2a:** Enantiomers that have energetic barriers values between 20 kcal·mol<sup>-1</sup> and 23 kcal·mol<sup>-1</sup>. These compounds can be clearly detected and sometimes resolved. the racemization process is too fast in fact, if you have the pure enantiomer, at most in 1 hour, it is completely racemized. For this reason, for most application the compounds can be considered a single entity.

- 2.2. Class 2b:** Enantiomers that have energetic barriers values between 23 kcal·mol<sup>-1</sup> and 30 kcal·mol<sup>-1</sup>. These compounds can be resolved and stored as a single enantiomerically pure atropisomer for hours or weeks at temperature of +25 °C.
- 3. Class 3:** Enantiomers that have energetic barriers values larger than 30 kcal·mol<sup>-1</sup>, with a half-life time in order of years. The single pure atropisomer are considered kinetically stable.

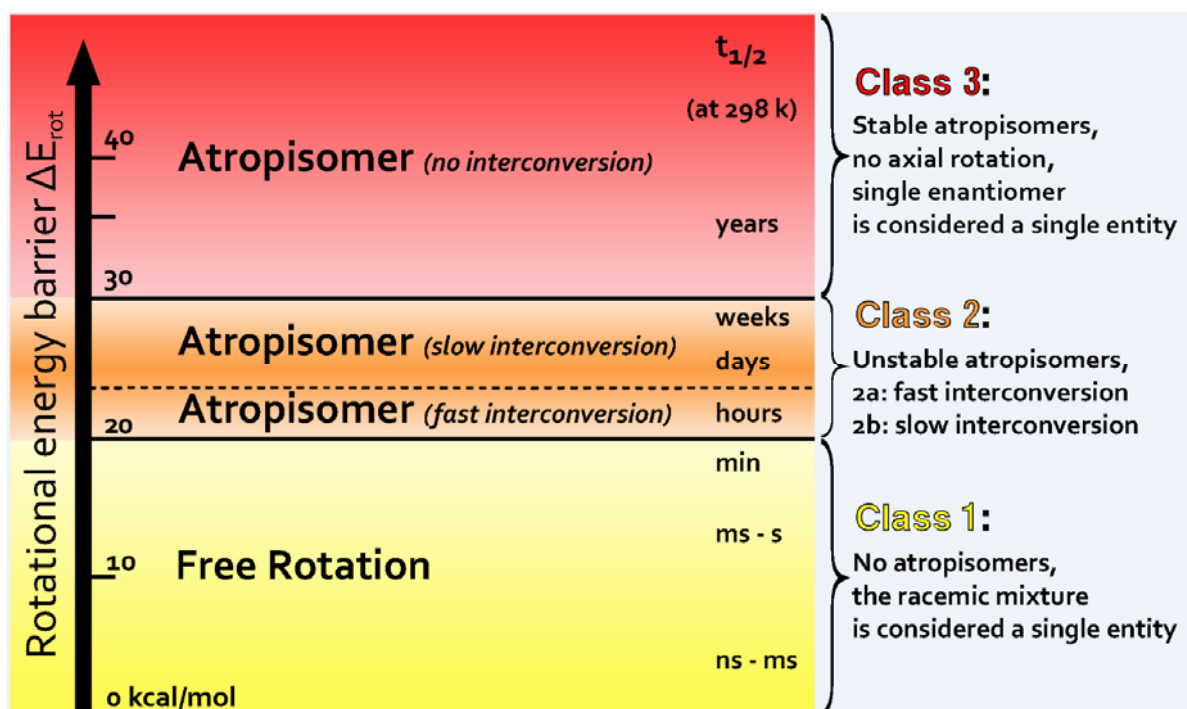


Figure 3. Rotational energy barrier with relative half-life time at + 25 °C of the single atropisomer.

This is not a rigid classification but there is a gradual passage from a class to another.

Finally, we need to make some consideration about this classification:

- The values of rotational barriers are lowest when the compounds are in solution then they are in solid state.
- Both in the crystalline and in the amorphous state, the rotational barrier is different, related to the packing of the crystalline structures.
- We consider the stability of atropisomers at room temperature, but as only kinetic process the rotation is highly influenced by temperature. As we will see better in conclusion the half-time life of a single atropisomer is inversely proportional to the temperature.

One peculiar feature is that they differ from other chiral compounds because it is often possible to obtain thermal equilibration starting from a single conformation. In fact, as the temperature increases, the molecule is supplied with sufficient energy to overcome the energy barrier ( $\Delta G^\ddagger$ ), generating free rotation around the bond and making indistinguishable the two atropisomers. Conversely, if they are indistinguishable, it is possible, by going to lower temperatures, to subtract energy from the molecule to make the energy barrier less accessible and thus be able to discriminate the two atropisomers. Another difference is that the compounds possess a stereogenic centre and that the nomenclature of the absolute configuration of the atropisomers is different from these. The absolute configuration of conformers is given using the concept of helicity that is based on the dihedral angle (Figure 4).

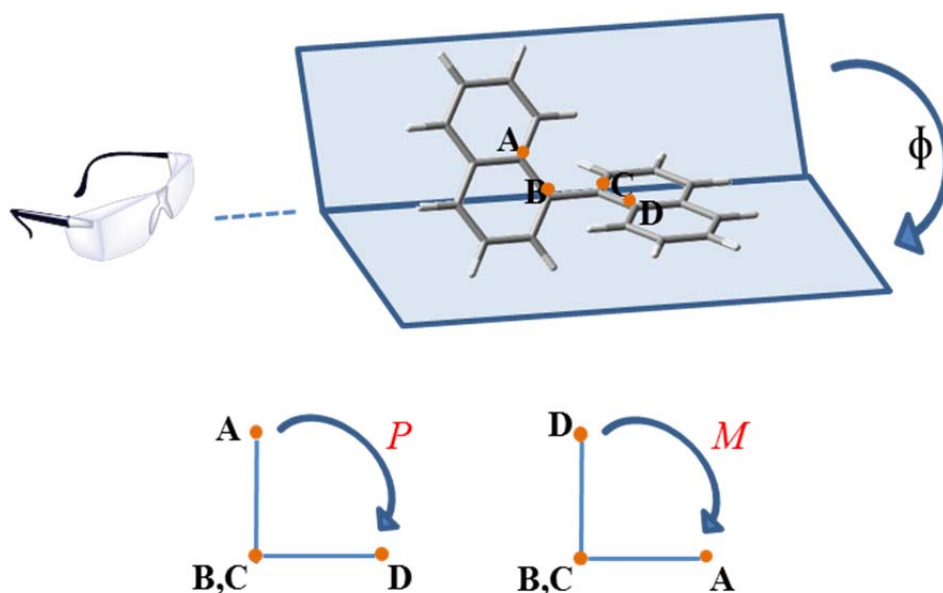


Figure 4. Schematic representation of the dihedral angle (up) and its nomenclature (bottom).

A dihedral angle ( $\phi$ ) is described by four points (A, B, C, D) and is obtained when two planes intersect along one side. The nomenclature is determined by looking at the **B-C** axis, by the substituent closest to the observer and having the highest priority (**A**) in the first plane, going towards the one having the highest priority (**D**) in the second plane and depending on the fact that this rotation is in clockwise or counter-clockwise we have the configuration **P** - plus (clockwise) or **M** - minus (counter-clockwise) direction.

In the twentieth century compounds containing chiral axes have been widely studied both for the discovery of new drugs and for the research of new catalysts for asymmetric synthesis. One of the most significant examples is BINAP, a chiral ligand used in enantioselective reactions (Figure 5).

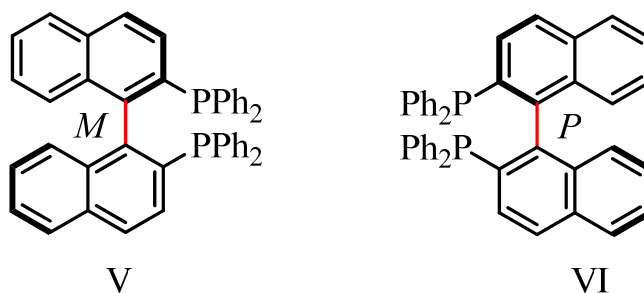


Figure 5. The two atropisomers of the BINAP.

The two atropisomers of BINAP are stable; this is due to the fact that, at room temperature, the rotational energy barrier, around the bond that coincides with the chiral axis, is so high as to prevent its rotation.

## 2. Aim of the thesis

The aim of this experimental thesis was to obtain and to characterise new molecules with boron-nitrogen bonds and with a boron-aryl chiral axis. In particular, we decided to study the 1,2-dibenzoazaborine. The prepared molecules are differently substituted in the *ortho* position of the aryl ring linked to boron (**5a**, **5b**, **5c** and **5d** in Figure 6).

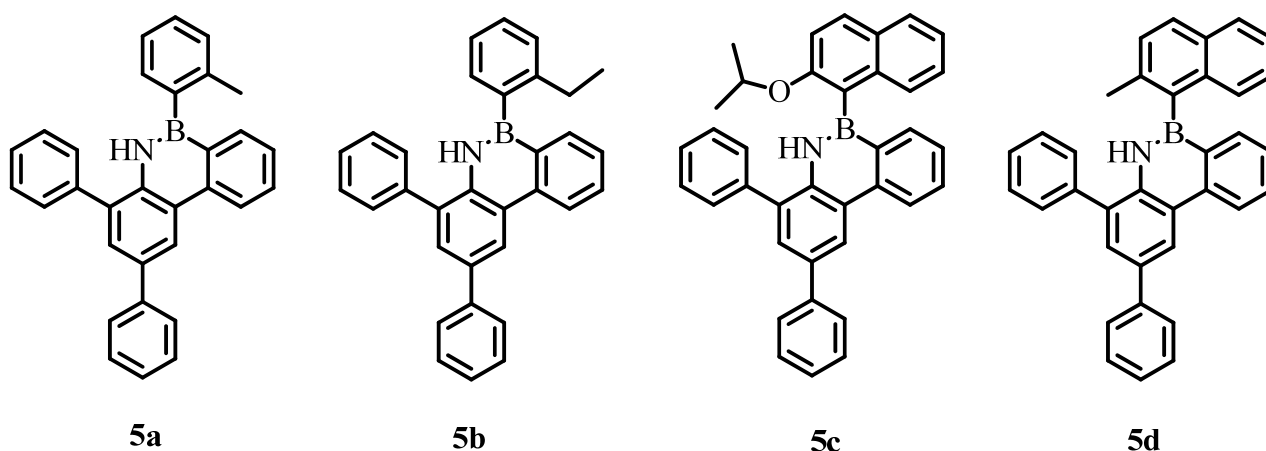


Figure 6. Synthesized compounds **5a-5d**.

These organic compounds have different rotational barriers depending on the steric hindrance in the *ortho* position that increases starting from **5a** to **5d**.

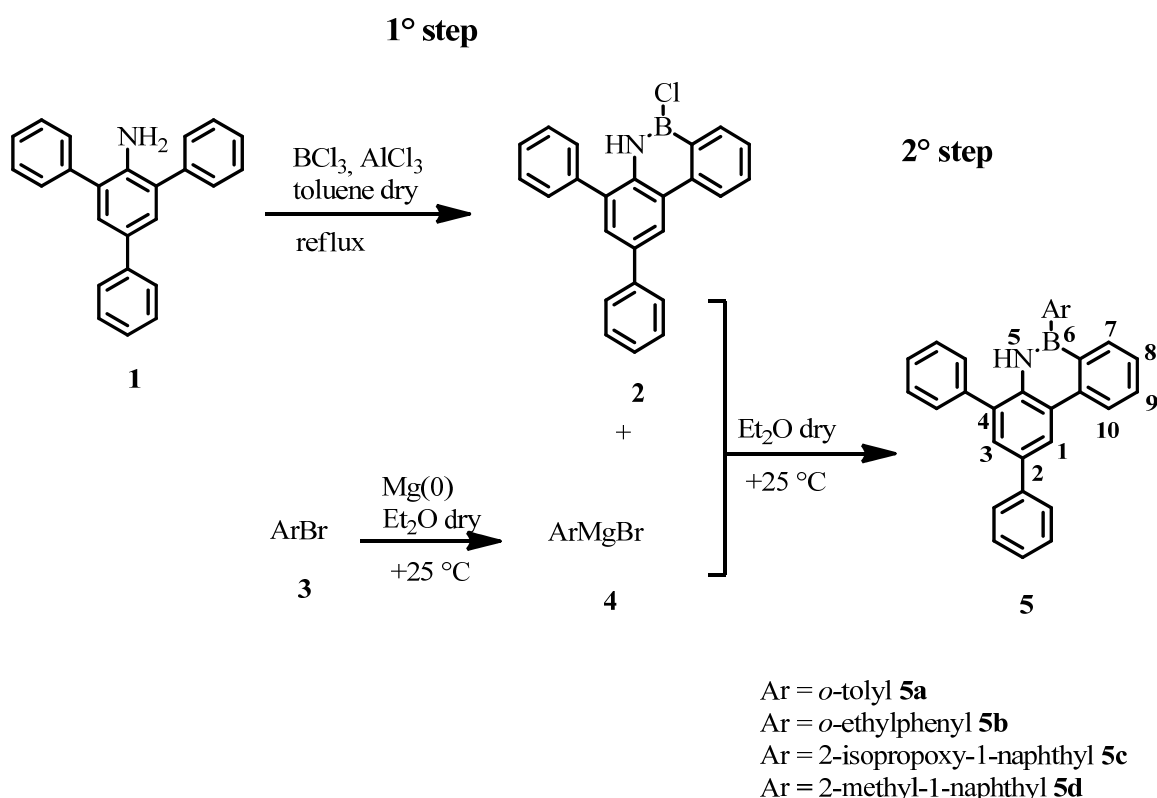
For the synthesized compounds the following analyses were carried out:

1. Computational study using DFT was performed in order to find the possible stable conformations, the relative free energies of the ground and transition states. Then they have been used to obtain the mechanism of interconversion and as support for subsequent experimental analyses.
2. Research of a synthetic way, of the conditions of purification of the products **5** and their optimization was done to obtain the products with good yields to carry out the various types of analysis. Their complete characterization was made using NMR spectroscopy and mass spectroscopy.

- 3.** Dynamic-NMR and Dynamic-HPLC were used for unstable atropisomers **5b** and **5c** respectively.
- 4.** Kinetic study aimed to obtaining the value of the experimental rotational barrier ( $\Delta G^\ddagger$ ) of the compound **5d** through thermal equilibration monitored by means of enantioselective dynamic-HPLC analysis.
- 5.** Determination of the absolute configuration of compound **5d** was done by comparison of experimental and calculated ECD.

### 3. Results and discussion

The first part of this project has been dedicated to the optimization of the synthetic route to the products of interest following a preparation that has been recently reported.<sup>10</sup> Being the aim of the work to study the energy barriers of 1,2-dibenzoazaborine, we stopped at the first part of the procedure reported (Scheme 1).



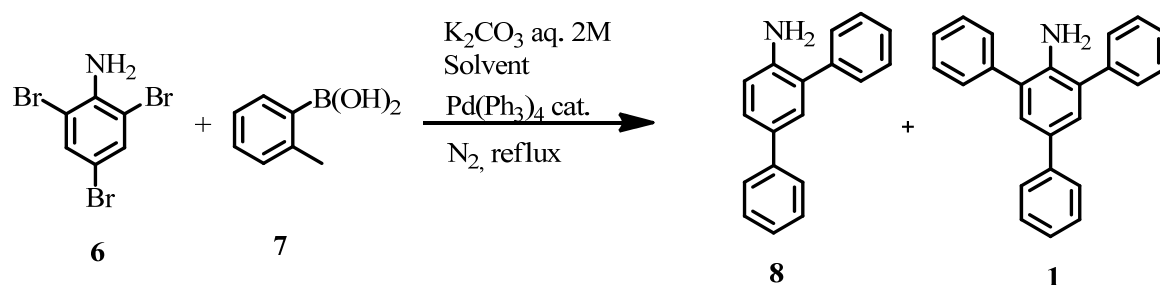
Scheme 1. Synthesis of 1,2-dibenzoazaborine **5**, and atom numbering of the final compound.

The pioneer of this type of reaction was Dewar, who reported the first synthesis of 9,10-azaboranphenantrene.<sup>11</sup> The key step is a Friedel-Crafts reaction that gives the intermediate product **2**, using BCl<sub>3</sub> and AlCl<sub>3</sub>. The use of different nucleophilic groups, *e.g.* Grignard reagents, allows the synthesis of the 1,2-dibenzoazaborine **5**. These types of reactions are usually done into a glovebox because the instability intermediate **2** in the air. To update this synthesis and to make it available to everyone without the glovebox,

we have tried to optimize a new procedure that allows us to obtain the desired product with good yields. In the next paragraphs are shown the various optimized reaction steps.

### 3.1 Synthesis of the 2,4,6-triphenylaniline 1

The starting tri-phenylaniline has been synthesized (Scheme 2) starting from 2,4,6-tribromo-aniline through the Suzuki Coupling reaction. This reaction is the palladium-catalysed cross coupling between organo-boronic acid and halides. It was first published in 1979 by Akira Suzuki and he shared the 2010 Nobel Prize in Chemistry<sup>12</sup> with Richard F. Heck and Eichi Negishi for their effort for discovery and development of palladium-catalyzed cross couplings in organic synthesis.<sup>13</sup>



Scheme 2. Synthetic scheme of Suzuki coupling reaction.

Table 1 shows the attempts made in optimizing this first reaction step.

Table 1: Yield of product obtained by Suzuki coupling reaction with different solvents

Solvent (0.1 M)	Yield (%) <b>1</b>	Yield (%) <b>8</b>
THF	<b>2</b>	-
Toluene/THF (1:1)	<b>11</b>	<b>7</b>
Tol/CPME (1:1)	<b>93</b>	<b>0</b>
Tol/CPME (19:1)	<b>90</b>	<b>0</b>

Preliminary experiments show that using only THF we obtained poor results, so we decided to use toluene and THF solution in 1:1 ratio, getting a better yield (11%) but also the by-product **8** was formed, as seen from the HPLC chromatogram (Figure 7).

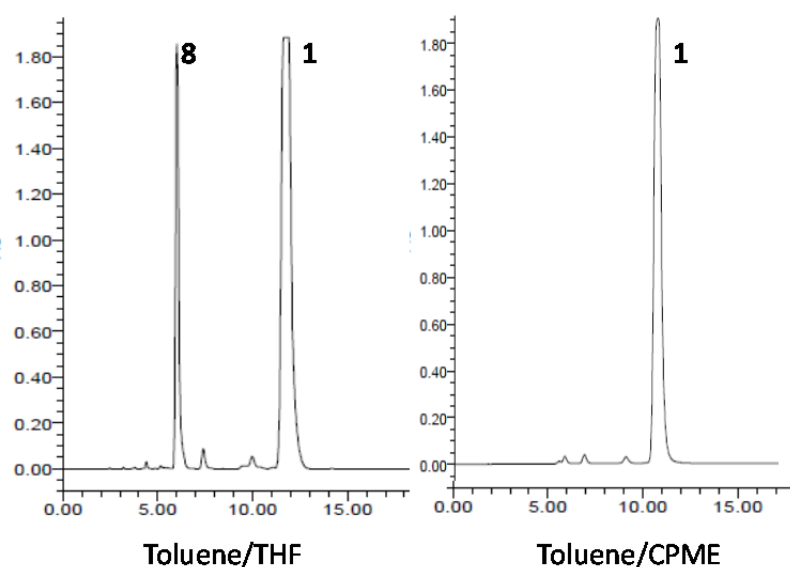


Figure 7. HPLC chromatograms of products **1** and **8**. (Luna-C18 (5 $\mu$  100 $\text{\AA}$ , 250 x 21.2 mm) with ACN:H<sub>2</sub>O in 90/10 ratio).

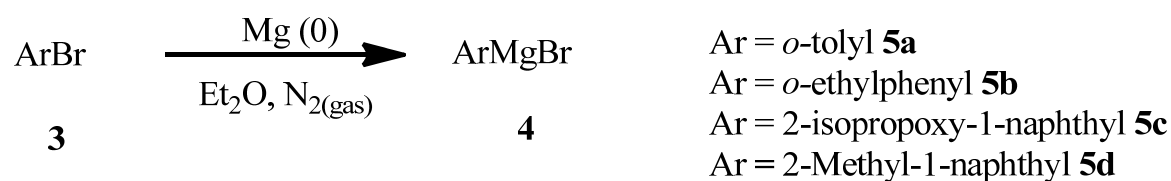
Since the tri-substituted and the bi-substituted products are difficult to separate without HPLC, we decided to change the solvent and use a 1:1 mixture of toluene and cyclopentylmethylether (CPME) because in literature it was reported<sup>14</sup> that with the use of CPME brings great improvements to the Suzuki reaction due to its affinity in the activation of boronic acids. From the experiments we see that, in this case the use of

CPME improves a lot the yields of the reaction. Moreover, when the amount of CPME was decrease, we have noted that a 19:1 ratio provides results practically equal to the previous test, with very good yields ( $\approx 90\%$ ). Most important thing is that the three phenyls are linked to 2,4,6-tribromoaniline, and no di-substituted or mono-substituted products have been obtained. In addition, there was the formation of a few by-products and the purification of the product has been done easy. In fact, we purified the product **1** by crystallization in acetonitrile, avoiding the use of HPLC and silica gel chromatography.

### 3.2 Optimization of synthesis of 1,2-dibenzoazaborine **5**

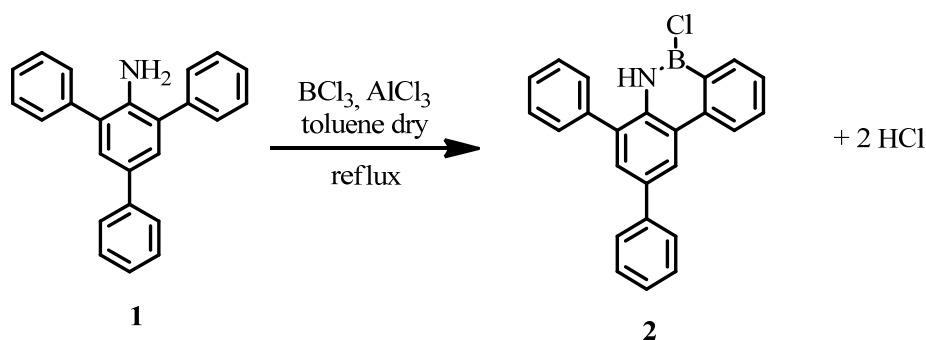
The optimization of the synthetic procedure was made on product **5a** which have the lowest steric hindrance. The synthetic route used is shown in Scheme 1, according to the reported procedure.

The reaction takes place in two steps: in the first step we have made the intermediate **2** and in the second step the Grignard reagent was added. The Grignard reagents prepared in the standard conditions are shown in the Scheme 3.



Scheme 3. Grignard reagents preparation.

The electrophilic borylation of one phenyl group was achieved using boron tri-chloride and aluminum tri-chloride (Scheme 4).



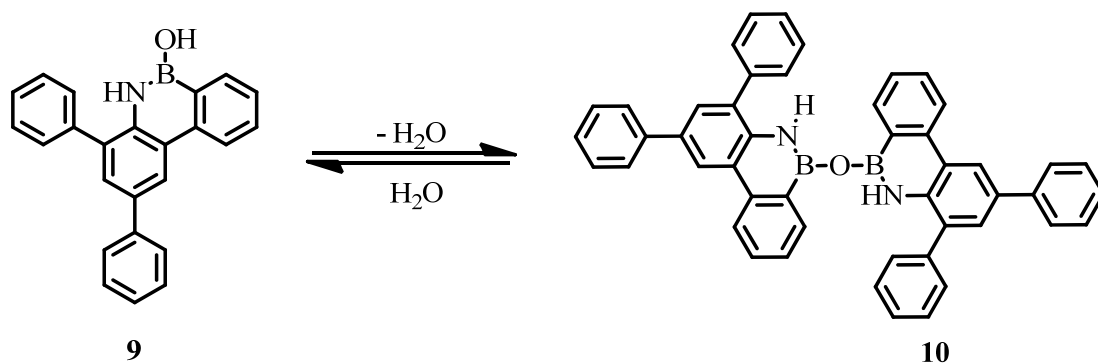
Scheme 4. First reaction step.

The derivative product **2** was not isolated due its instability and to avoid the use of glovebox we tried to do the next reaction in situ. Moreover, to eliminate the HCl and the  $\text{BCl}_3$  excess, the mixture was kept on vacuum until no gas was present in the reaction apparatus.

At this point, the second reaction step, on Scheme 1, has been tried with three different approaches:

- 1) The Grignard reagents in dry ethyl ether solution were directly added dropwise to toluene mixture of intermediate **2**.
- 2) The intermediate **2** was dried at vacuum and dissolved again in dry toluene before the addiction of the Grignard reagent.
- 3) The intermediate **2** was dried at vacuum and dissolved in dry ethyl ether before the addiction of the Grignard reagent.

The first test did not yield good results: no trace of the product can be seen by NMR analysis of the crude product. Most probably the HCl formed remain dissolved in toluene and reacts with the Grignard reagent. Moreover, any traces of water gives easy hydrolysis of intermediate **2** yielding the hydroxyl derivate (**9**) that can be in equilibrium with the oxide (**10**) as shown in the Scheme 5.<sup>15</sup>

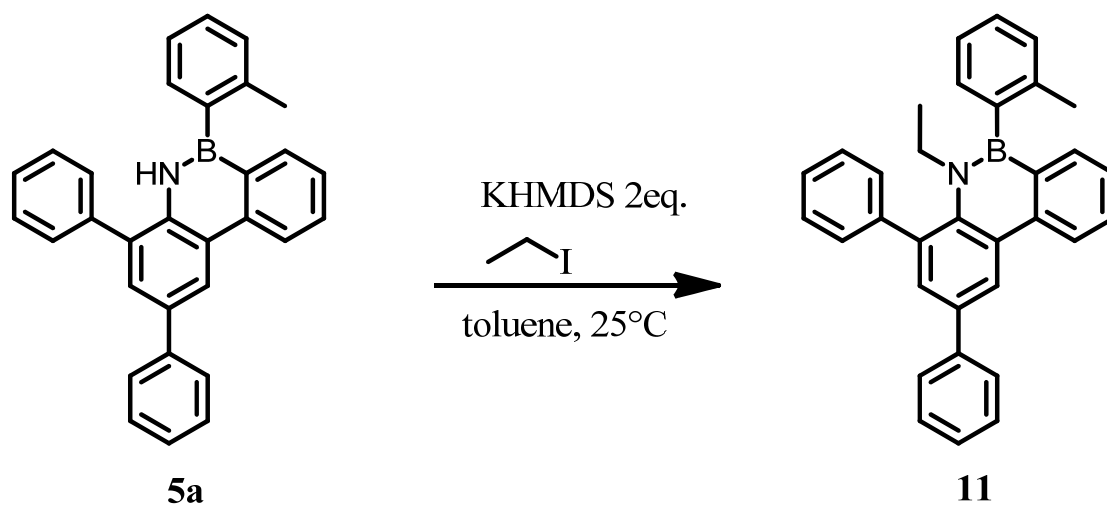


Scheme 5. Equilibrium hydroxyl **9** and oxide **10** derivatives.

As reported in literature by Dewar,<sup>16</sup> also the compound **10** can react with the Grignard reagent, so the main problem of this procedure has to be found in the presence of HCl. To avoid the presence of HCl and H<sub>2</sub>O (entries 2 and 3), the solvent of the first step was removed as azeotrope toluene/water at the vacuum pump, obtaining a green solid mixture of compound **2** and **10** (if water was present). The solid was then dissolved again in dry toluene, obtaining a biphasic mixture with the Grignard ethyl ether solution. In these conditions we obtained the desired product **5a** but with a low yield (5%). So, in the third attempt we used only fresh prepared dry ethyl ether freshly prepared for the second step, to avoid the biphasic mixture. In this way the yield increased significantly to 31%. The reaction crude was purified with a silica column and then by means of reverse phase HPLC (Luna C18 column). This procedure was then used to prepare all the compounds **5b**, **5c** and **5d**.

### 3.3 Attempts of synthesis of 1,2-dibenzoazaborinine **11**

Following the synthesis of the compound **5a** we thought to insert a chiral probe on the nitrogen atom to obtain compound **11** as show in Scheme 6. The chiral probe is necessary to follow the dynamic process with NMR.



Scheme 6. Synthetic route of compound **11**.

The deprotonation of the NH was achieved with the strong bases KHMDS or TMEDA/*n*-BuLi. The success key of this procedure is the utilization of a very strong and sterically hindered base<sup>17</sup> not nucleophilic, because the nucleophilic can degrade the product. In fact, the tolyl can be replaced by the base by nucleophilic substitution. Unfortunately the reaction mixture was very complex and unworkable because the very strong base fragmented the starting molecule.

### **3.4 Synthesis of 1,2-dibenzoazaborine 5b**

Since the attempt to insert a chiral probe on nitrogen was unsuccessful, we decided to insert an ethyl group, as chiral probe, directly on the aryl linked to the boron center. Like the first product **5a**, in this case we managed to purify product **5b** with a flash chromatography column (petroleum ether/DCM, 9.5:0.5, followed by further purification by preparative reverse phase HPLC Synergi 4 $\mu$  Polar – RP 80Å column. The product is a white solid and it was obtained with a 32% of yield.

### **3.5 Conformational studies of 1,2-dibenzoazaborine 5b**

The 1,2-dibenzoazaborine with different asymmetric aryl group bonded to the boron atom, generate a pair of atropisomers, because the substituent bonded to the aryl group is driven out of the plane of the aromatic scaffold of the rest of the molecule. Thanks to the 180° rotation around the chiral axis we can go from one atropisomer to another (Figure 5). The stability of these conformational isomers depends by the substituents steric hindrance due to the electronic repulsion with the electronic clouds of the other molecular fragments. If there is a large steric hindrance the two atropisomers will be stable, if not the resulting conformations will be stereolabile.

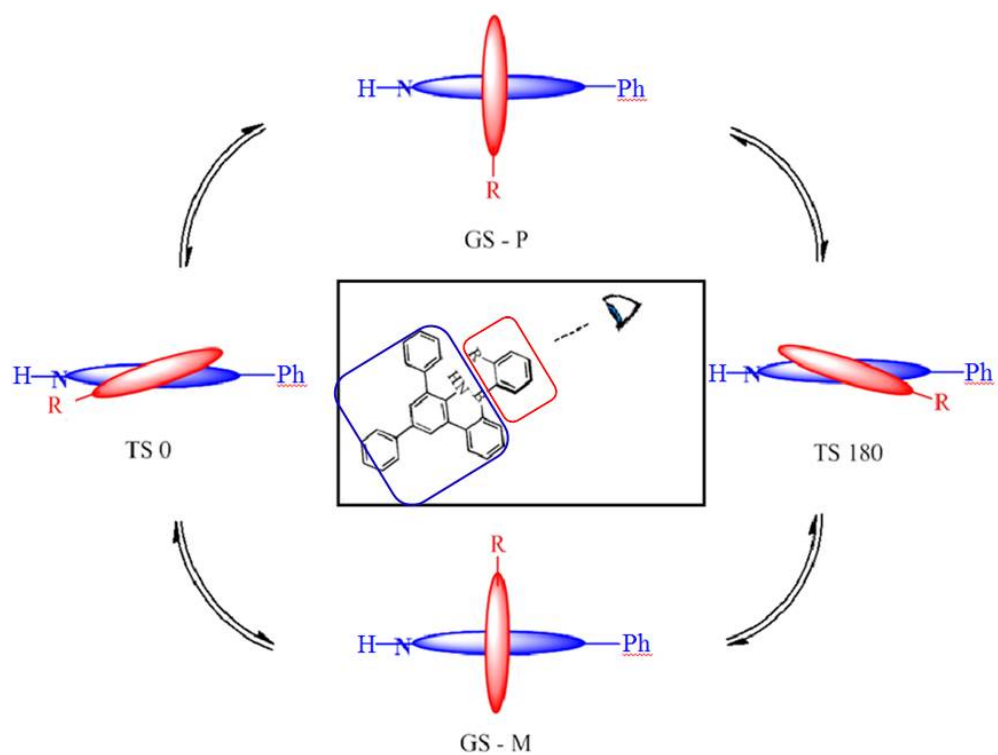


Figure 5: Rotation around the chiral axis.

To understand if the conformations will be stable or stereolabile, we can calculate the rotational barrier energy by DFT method. All molecules can take many conformations but only some of them are actually populated. The four most stable conformations relative to *M* atropisomer of compound **5b** are shown in the Figure 6, and Table 1 reports the energy values for both ground and transition states, regarding the *M* configuration.

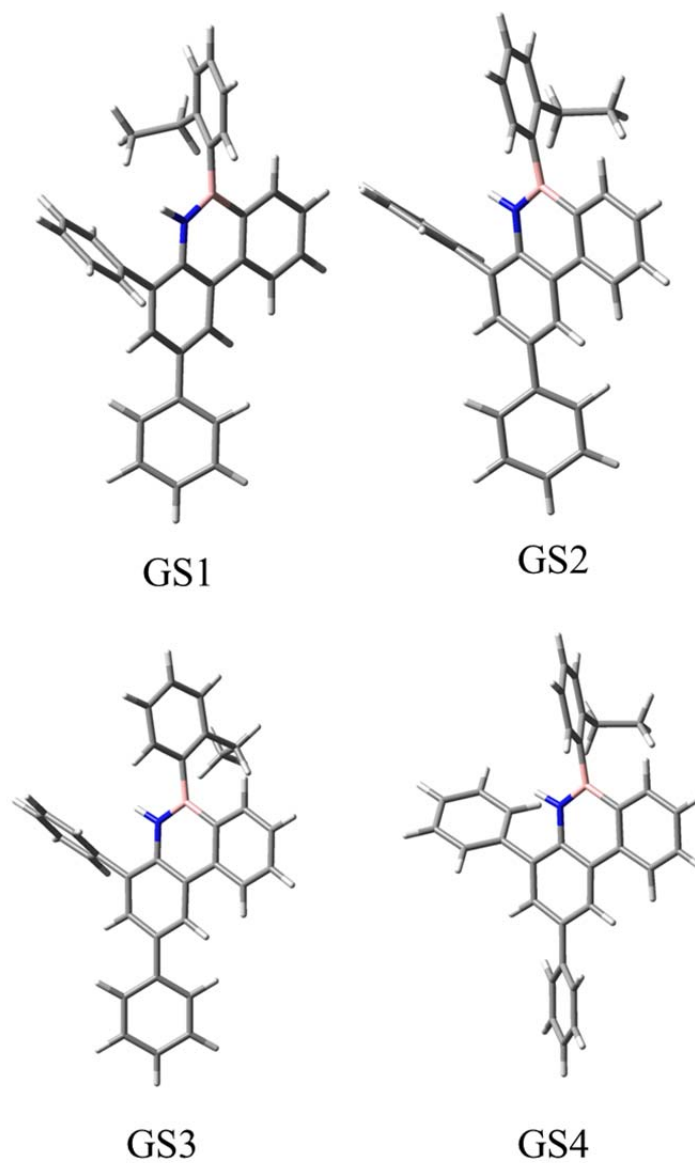


Figure 6. Four major populated conformations of compound **5b**.

The four ground states have very small energy differences; this implies that all conformations should be appreciably populated. They differ from each other's for the orientation of phenyls bonded on the position 2 and 4 of the di-benzyl system or for the orientation of the ethyl group on *ortho* phenyl bonded to the boron atom. The energy values of the transition states were calculated with respect to the global minimum (GS3 conformation). The two conformations relative to the TS are shown in the Figure 7.

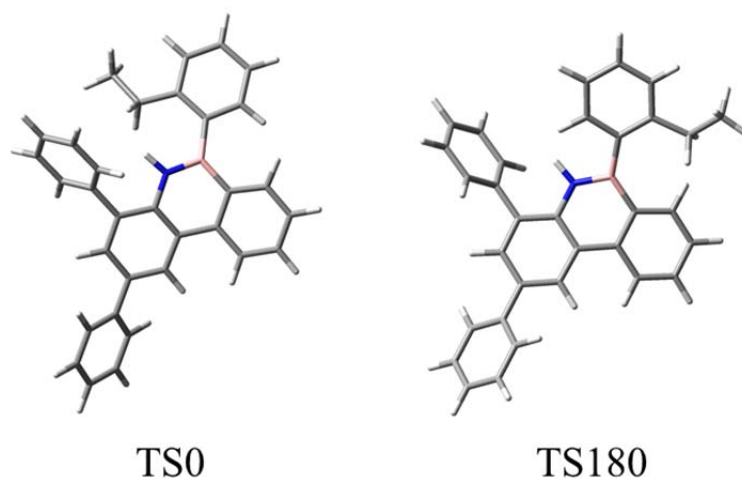


Figure 7. Transition states conformations of **5b**.

The transition state represents the crossing between two ground states and it is the point with highest energy in the conformation interconversion path. In these transition states the aryl is almost planar with the rest of the molecular scaffold and the *ortho* substituent of the aryl group can rotate over the nitrogen atom (TS0) or in the opposite site (TS180). The minimum value calculated of transition states (TS180) is the free energy rotational barrier that can be compared with the experimental  $\Delta G^\ddagger$ .

Table 2: Optimized ground and transition states normalized of the *M* conformations in kcal·mol<sup>-1</sup>, calculated at B3LYP/6-31G(d) level.

Entry	GS1	GS2	GS3	GS4	TS0	TS180
	$\Phi^a$	$\Phi^a$	$\Phi^a$	$\Phi^a$		
	(%) <sup>b</sup>	(%) <sup>b</sup>	(%) <sup>b</sup>	(%) <sup>b</sup>		
<b>5b</b>	0.008	0.098	0.000	0.199	13.238	18.248
	-112.3°	-68.2°	-112.1°	-68.9°		
	26.2%	22.4%	26.5%	18.9%		

a: Dihedral angle values

b: Percentage of each populated state

To determine the experimental  $\Delta G^\ddagger$  the compound **5b** was studied by means of variable temperature NMR spectroscopy (Figure 8, left), following the evolution of the ethyl signal. In fact, the CH<sub>2</sub> display different multiplicity depending on the rotational rate. When the rotation of the group on B-C<sub>aryl</sub> bond is fast in the NMR timescale a quartet is visible on the spectrum at +25 °C. When the temperature is decreased, the rotation becomes slow in the NMR timescale and the CH<sub>2</sub> displays at first an enlargement of the linewidth, until the coalescence at -15 °C. Below this temperature two set of broaden signals are visible and eventually, two definite signals are visible at the -60 °C. This means the two enantiomeric conformations are stable at this temperature in the NMR time scale.

By line shape simulation of the Dynamic-NMR spectra (Figure 8, right) through a mathematical model we obtained the rate constants for the dynamic process, and hence the  $\Delta G^\ddagger$ . The program used for this simulation is DNMR-6 QCPE n°633 (Dynamic Nuclear magnetic Resonance - Quantum Chemistry Program Exchange). The program simulates the theoretical NMR spectra as the kinetic constant ( $k_{TC}$ ) varies, and then compares them with the experimental ones in order to obtain the value of the  $\Delta G^\ddagger$  at different temperature. As we can see in the Figure 6, the  $\Delta G^\ddagger$  found through this type of system is 12.6 kcal·mol<sup>-1</sup>, which is quite close to TS0 (13.2 kcal·mol<sup>-1</sup>), theoretically calculated with the DFT method.

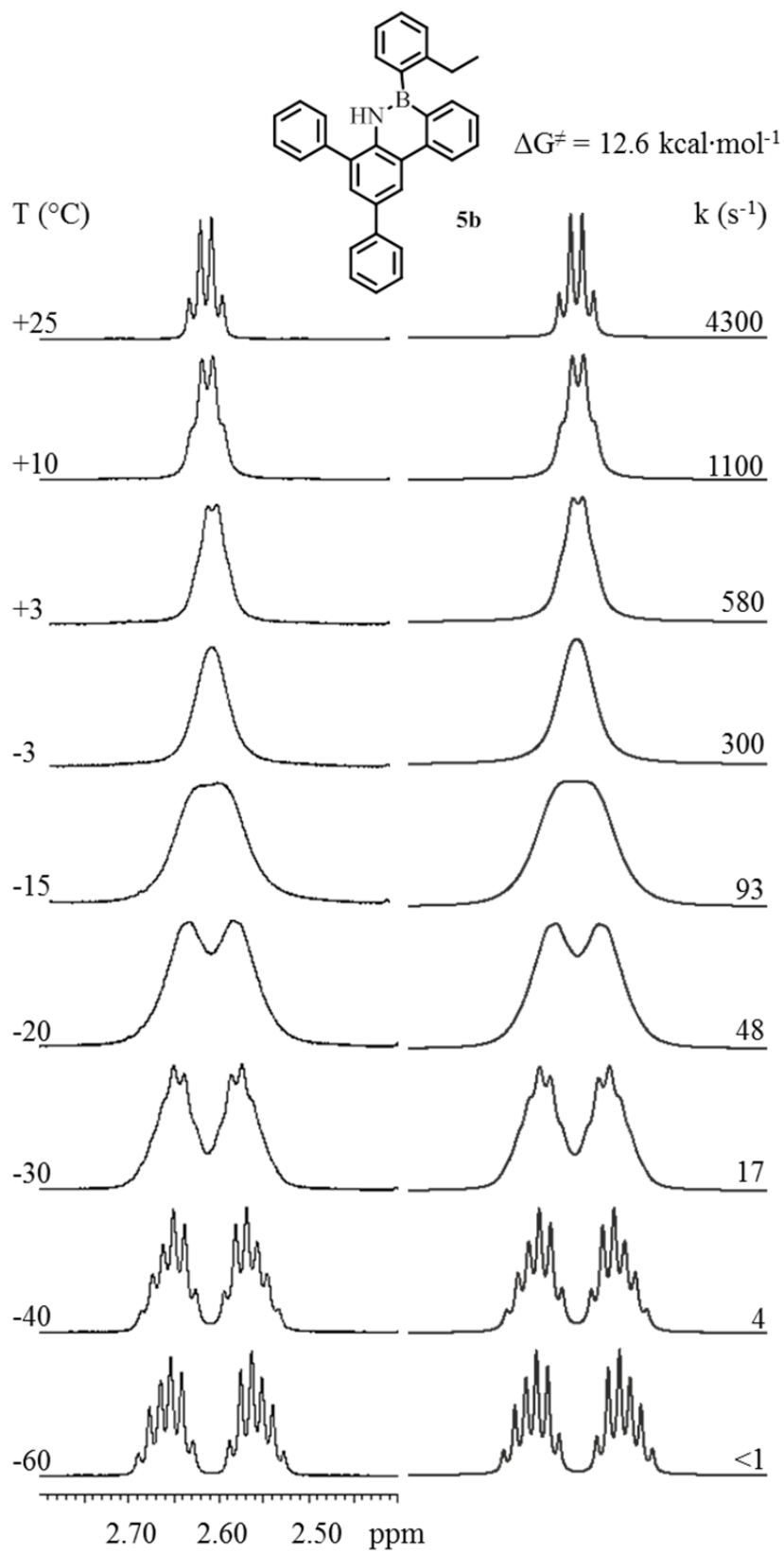


Figure 8. NMR spectroscopy at variable temperature (VT).

### 3.6 Synthesis of 1,2-dibenzoazaborinine **5c**

Compound **5c** was synthesized because we tried to find a product with a high rotational energy barrier in order to have stable. Like two others, this compound (**5c**) is synthesized on the base of the compound **5a** too (Scheme 6) and like the product **5b** we managed to separate easily the product to the rest of the reaction mixture with a flash chromatography column (Petroleum ether/DCM - 9.5:0.5) obtaining a yield of 36%.

Also in this case we insert the chiral probe directly on the molecular fragment linked to the boron center. To characterize compound **5c** by dynamic NMR we have purified the product by preparative HPLC with Synergi 4u Polar – RP 80Å column as the compound **5b**.

### 3.7 Conformational and kinetic studies of 1,2-dibenzoazaborines **5c**

Compound **5c** have a higher steric hindrance respect **5b** due to the naphthyl group and the *iso*-propoxy in *ortho* position and atropisomers could be made. Therefore, to forecast if the compound **5c** will be really stable or stereolabile, we can calculate the rotational barrier energy by DFT method. The four ground state conformations relative to the *P* atropisomer are shown in Figure 9.

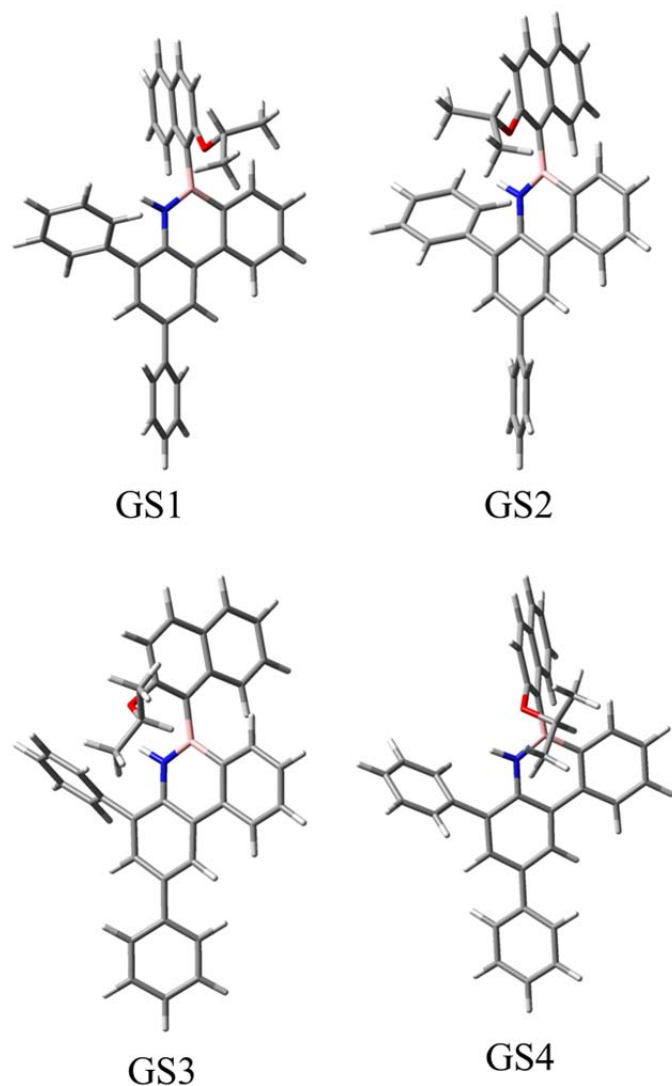


Figure 9. Compound **5c**, ground states conformations.

As shown in Table 3, the ground state that has the minimum energy values is GS1. In this case the two phenyls and the boron-linked naphthyl are oriented perpendicular to the rest of the molecular scaffold. Due to the difficult to determinate the transition states for the big steric hindrance, a scanning Potential Energy Surfaces (PES) was performed to find the geometry of the TS structure. This computational method consists in a series of calculations performed in which one of the structural parameters is fixed to a certain value, while all other parameters are optimized to their most favorable values. Therefore, starting to *P* conformation the dihedral angle was rotated of 20° for each step obtaining the PES shown in Figure 10.

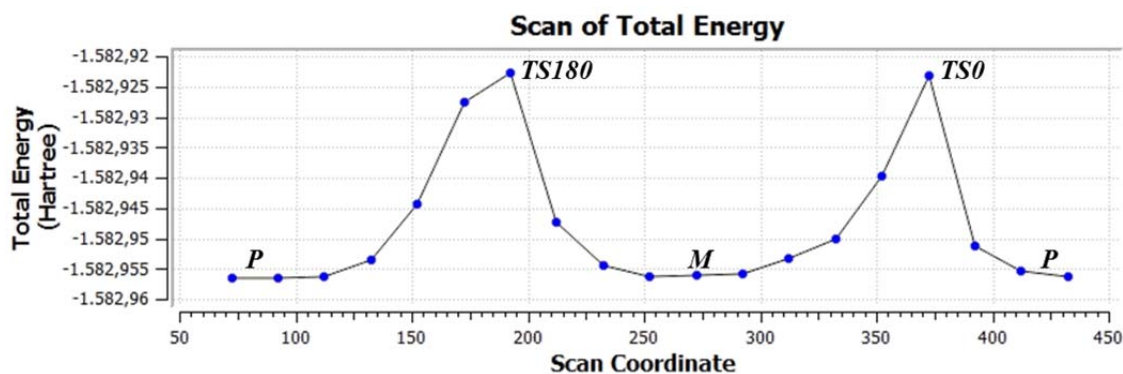


Figure 10. Diagram Scanning Potential Energy Surfaces of compound **5c**.

After this the two points with the bigger energy, TS0 and TS180 were optimized by DFT method and shown in Figure 11. The computational of vibrational frequency for this two transition states shows the presence of a single imaginary frequency, that confirms they are true TS. As we can see by the Table 3, the TS0 is the higher energy conformation so the experimental results will be compared with the TS180.

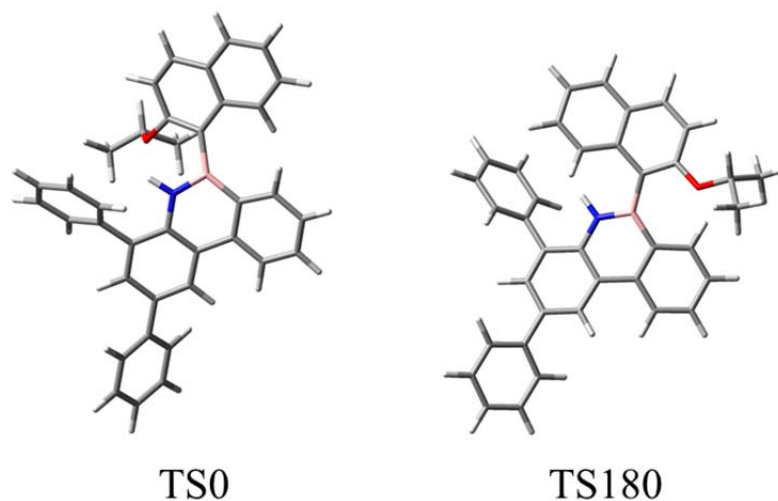


Figure 11. Compound **5c**, transition states conformations.

From the initial calculations made with the DFT method, energy equal to  $21.5 \text{ kcal}\cdot\text{mol}^{-1}$  is obtained. Therefore, already with this result we supposed that the molecule could be at the limit of stability at room temperature, which is then confirmed by the experimental results. A rotational barrier with this energy value it is above the limit of the Dynamic-NMR, and the Dynamic HPLC but this last one technique is probably more suitable. In

fact, D-NMR showed there was not exchange between the isopropyl CH<sub>3</sub> signal up to +120 °C.

Table 3. Optimized ground and transition states normalized of the *P* conformations in kcal·mol<sup>-1</sup>, calculated at B3LYP/6-31G(d) level.

Entry	GS1	GS2	GS3	GS4	TS0	TS180
	$\phi^a$	$\phi^a$	$\phi^a$	$\phi^a$		
	(%) <sup>b</sup>	(%) <sup>b</sup>	(%) <sup>b</sup>	(%) <sup>b</sup>		
5c	0.000	0.006	0.961	1.284	24.209	21.465
	+79.4°	+105.2°	+66.5°	+63.5°		
	43.4%	42.9%	8.6%	4.9%		

a: Dihedral angle values

b: Percentage of each populated state

Therefore, the compound **5c** was analyzed by D-HPLC. The column used is the ChiralPak AD-H, with eluent *n*-hexane/*iso*-propanol 95:5, and 1 mL·min<sup>-1</sup>. The chromatographic runs were done at different temperatures, from +15 °C up to +45 °C (continuous cyan line in Figure 12). At +25 °C we can see a ‘plateau’ between the two peaks, indicating that the two atropisomes are not stable at room temperature so we cannot separate them without lowering the temperature.

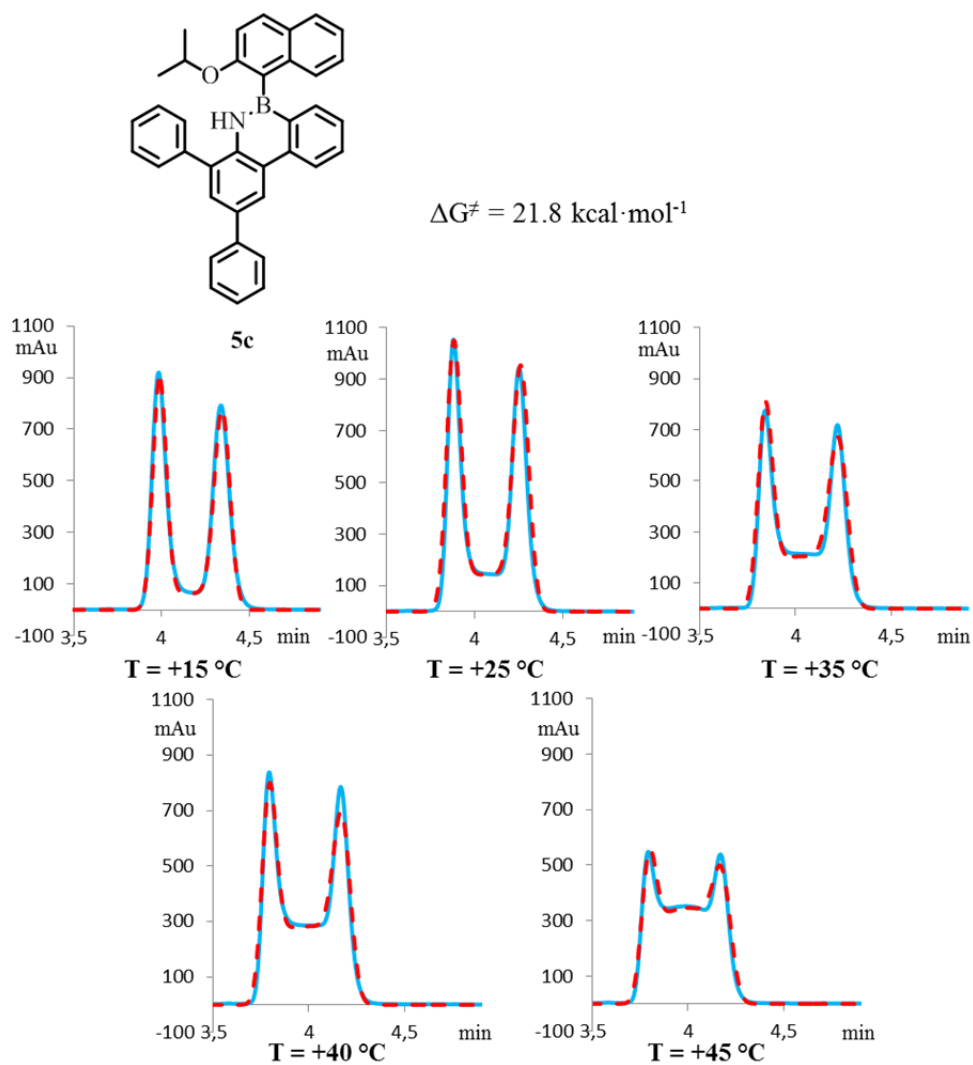


Figure 12. D-HPLC analysis performed on compound **5c**.

Table 4. Kinetic constants and free energy barriers at each temperature of compound **5c**.

Temperature (°C)	$k$ (s <sup>-1</sup> )	$\Delta G^\ddagger$ (kcal·mol <sup>-1</sup> )
+15	$5.3 \cdot 10^{-4}$	21.15
+25	$1.0 \cdot 10^{-3}$	21.52
+35	$2.0 \cdot 10^{-3}$	21.85
+40	$2.7 \cdot 10^{-3}$	22.03
+45	$4.4 \cdot 10^{-3}$	22.09

Once the temperature is decreased to +15 °C, the rotation is slower, but a lower ‘‘plateau’’ is still visible. On the other hand, the height of the plateau increases with the temperature, until the stereodynamic process has a faster rate and the separation is not possible. Analogously to the D-NMR, in the D-HPLC the kinetic constant is evaluated through line shape simulation of the chromatograms recorded at different temperature (dashed red line in Figure 12). Although different methods can be applied to reproduce the line shape (theoretical plate model,<sup>18</sup> continuous flow model<sup>19</sup>) one of the most reliable is the stochastic model,<sup>20</sup> where the separation is described through a time dependent function that can be simulated with appropriate software. The Model provides the kinetic rate constants at different temperatures, and the  $\Delta G^\ddagger$  was derived by Eyring equation obtaining a value of 21.8 kcal·mol<sup>-1</sup>.

Using a different approach, the rotational energy barrier was measured using kinetic studies with ECD methods. At room temperature, the compound stereo-lability did not allow us to separate the two atropisomers, so we separated the two keeping the column at a temperature of about +10 °C through a polystyrene envelope, poured with liquid nitrogen, and keeping the solvent pipes cooled with ice baths (Figure 13).



Figure 13. Photos of low temperature HPLC system.

All the eluted fractions were then cooled to 0° to preserve the enantiomeric purity. In this way we were able to separate the two atropisomers and then proceed with ECD kinetic studies.

After a rapid ECD scan to select the highest band value (mdeg), we set the polarized radiation to 230 nm, and a scan per second on the single point for an hour was done. Kinetic studies were performed at two different temperature, +19.7 °C and +25.4 °C (a thermocouple was put close to the cuvette to monitor the temperature) and the racemization was monitored observing the decrease of ECD signal over time (Figure 14-up).

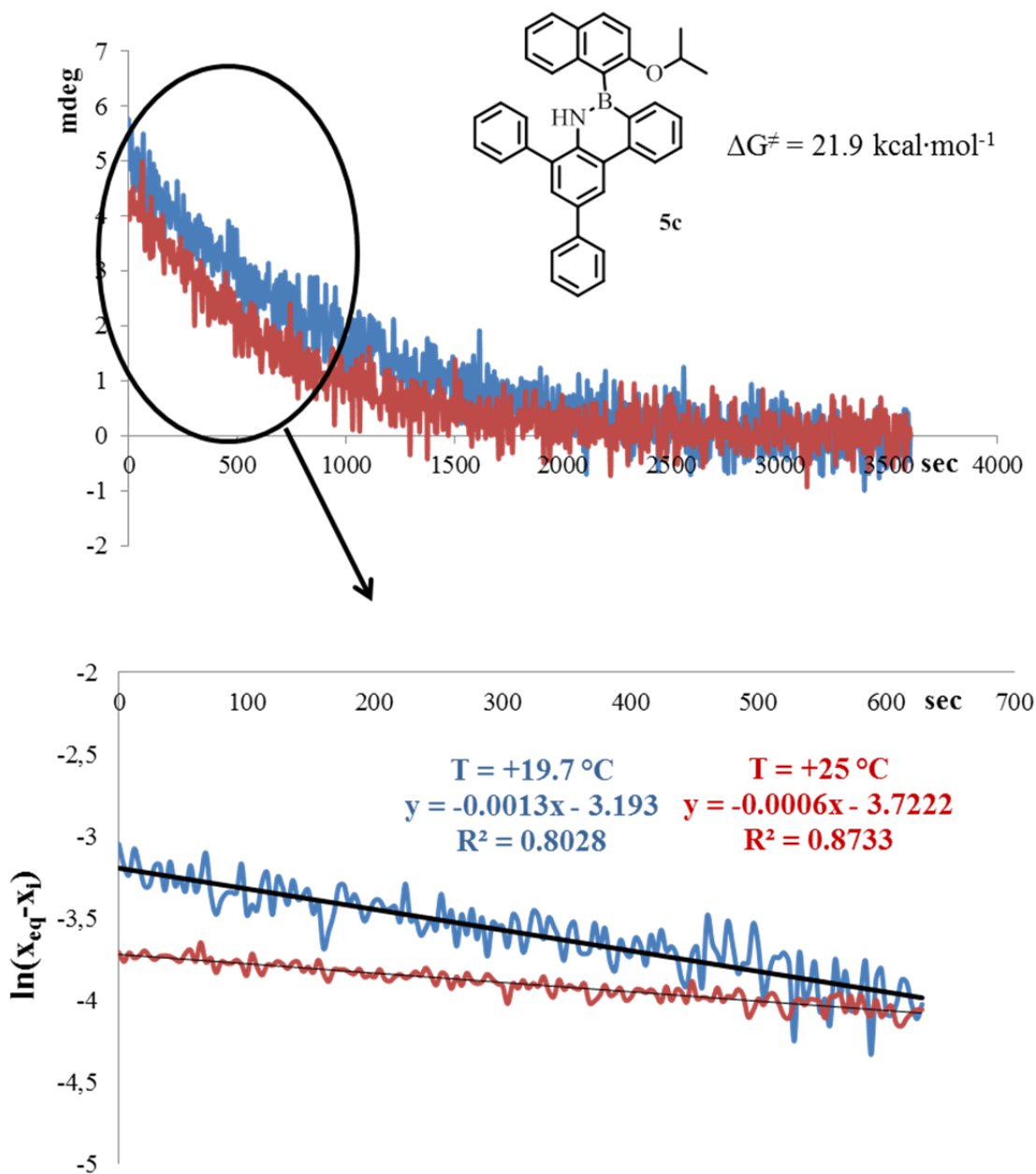


Figure 14. Up: racemization lines trend. Bottom: interpolation of obtained data.

Afterwards, the data obtained was mathematically interpolated through a series of equations which relate the kinetic constant with the molar fraction ( $x_i$ ) and the time (Figure 14 bottom).

The line equation is the following:

$$\ln(x_{eq} - x_i) = -2kt + \ln(x_{eq})$$

The molar fraction is defined as

$$x_i = \frac{(mdeg_{max} - mdeg_i)}{(2mdeg_{max})}$$

The equilibrium molar fraction is:  $x_{eq} = 0.5$

The mediated resulting kinetic constant is  $2.4 \cdot 10^{-4} \text{ s}^{-1}$ , with  $\Delta G^\ddagger = 21.9 \text{ kcal}\cdot\text{mol}^{-1}$ . This value is in agreement with that obtained with line-shape simulation of the dynamic-HPLC chromatogram.

### 3.8 Synthesis of 1,2-dibenzoazaborinine 5d

Compound **5d** was synthesized because with the analysis of compound **5c** made by dynamic HPLC. We were at the energetic limit in order to define stable the rotational energy barrier of the product at room temperature. This not makes to separate the two conformers at room temperature, so we can't analyze them by ECD to give their respective absolute configuration. So, due the methyl group is bigger than oxygen atom,<sup>21</sup> it will be created a major steric hindrance and, consequently, a bigger rotational energy barrier. The synthetic route was made on the base of the others compound like is show in the Scheme 1. We have separated easily the product to the rest of the reaction mixture with a flash chromatography column (petroleum ether/DCM, 9.5:0.5) and we have purified it by HPLC with Synergi 4 $\mu$  Polar – RP 80Å column.

### 3.9 Conformational studies of 1,2-azaborines 5d

Given the results obtained for compound **5c**, we changed the substituent in position 2 of naphthalene. In fact the methyl group provides bigger steric hindrance than the oxygen atom in the *iso*-propoxy group. In this way, the steric hindrance will be larger compared to compound **5c** and the barrier to racemization should raise. In this case, therefore, we should be able to separate the two atropisomers and to assign their absolute

configuration. Also for this compound we can calculate the rotational barrier energy by DFT method and the values obtained were compared with experimental results. The four conformations relative to *M* atropisomer are shown in the Figure 15 and Table 5 shows that the ground state with lowest energy is GS2. Like the others, also in this case we see that the substituents linked to the 1,2-dibenzoazaborine are positioned in a perpendicular way respect to the central structure of the molecule.

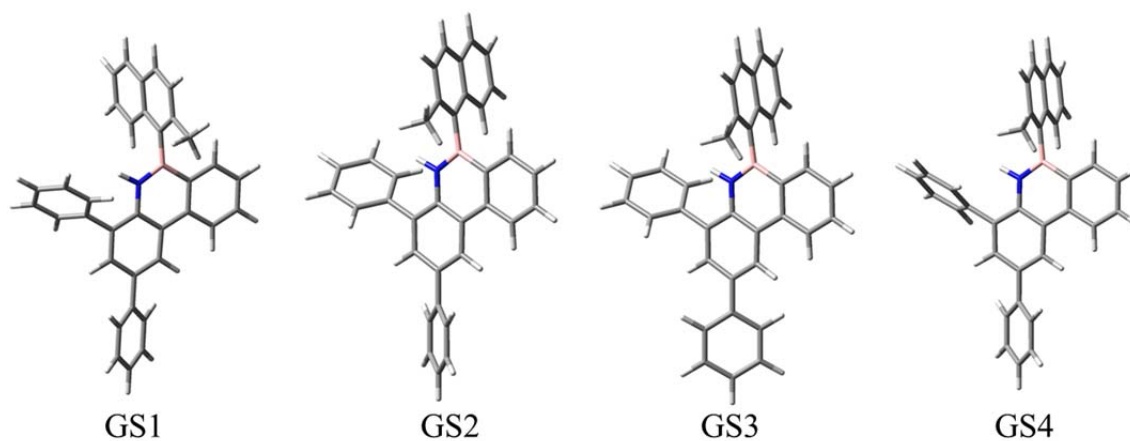


Figure 15. Ground states conformations of compound **5d**.

The two conformations relative to the TS are shown in Figure 16. The transition state with lowest energy is TS180.

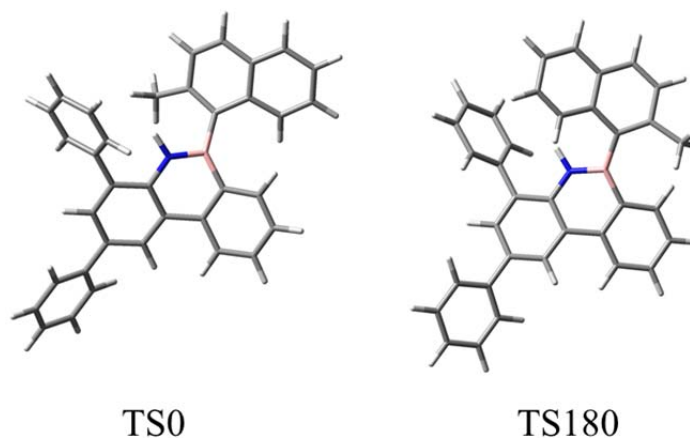


Figure 16. Transition states conformations of compound **5d**.

Table 5. Optimized ground and transition states normalized of the *M* conformations of compound **5d** in kcal·mol<sup>-1</sup>, calculated at B3LYP/6-31G(d) level.

Entry	GS1	GS2	GS3	GS4	TS0	TS180
	$\Phi^a$	$\Phi^a$	$\Phi^a$	$\Phi^a$		
	(%) <sup>b</sup>	(%) <sup>b</sup>	(%) <sup>b</sup>	(%) <sup>b</sup>		
<b>5d</b>	0.133	0.000	0.048	0.177	25.743	25.288
	-81.2°	-81.8°	-81.6°	-81.5°		
	23.1%	28.9%	26.6%	2.1%		

a: Dihedral angle values

b: Percentage of each populated state

The column used for the enantioselective HPLC was the analytic ChiralPak AD–H (0.75 mL/min) and solvent mixture was *n*-hexane/*iso*-propanol in 97:3 ratio. The chromatogram in Figure 17 was done at room temperature, showing the absence of any plateau. According to the theoretical results (Table 5), we can say that the atropisomers are stable at room temperature and therefore they are physically separable.

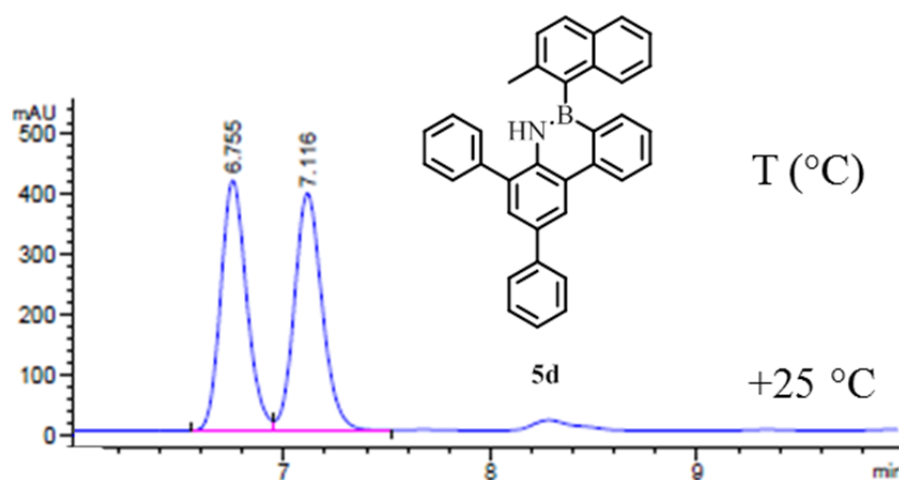


Figure 17. HPLC chromatogram spectrum of compound **5d**.

To purify each atropisomers we used the preparative ChiralPak AD–H column (2 cmϕ x 25 cm, 13 mL/min) with the same conditions see above. Once purified, the atropisomers was subjected to kinetic studies at different temperatures to obtain the experimental value of the energy barrier of racemization. The kinetic analysis was performed using three aliquots of first eluted enantiomer at three different temperatures. The aliquots were heated in an oil bath, a thermocouple was used to keep the temperature controlled and it was surrounded directly in the solvent. Samples were taken at different times and the atropisomerization process was followed by analytical enantioselective HPLC (Figure 18).

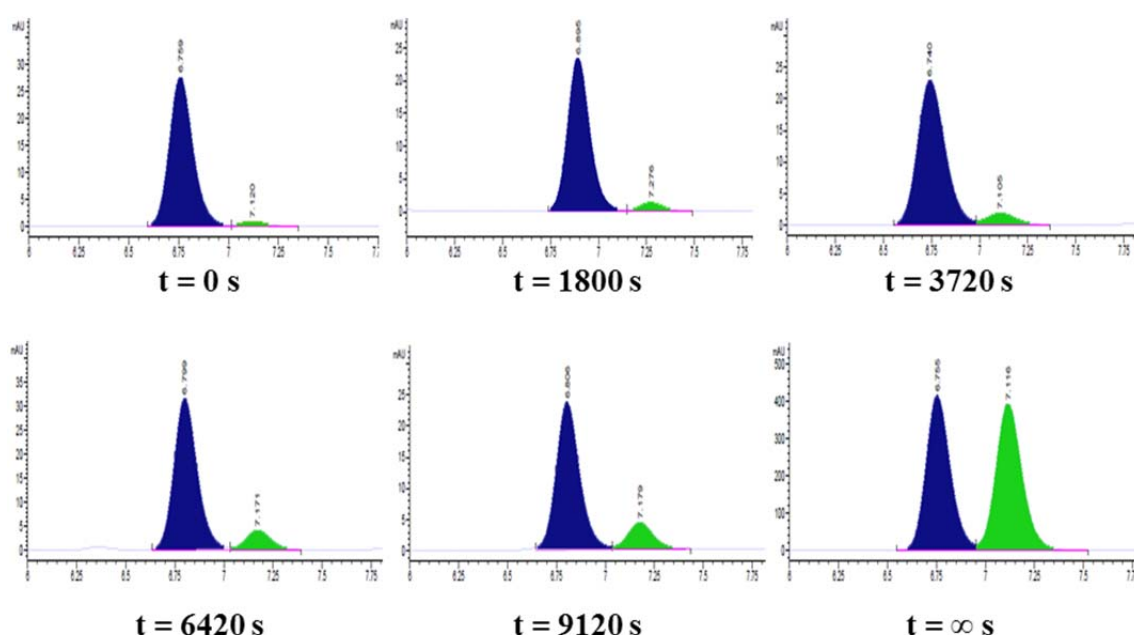
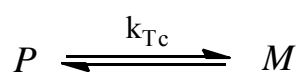


Figure 18. Racemization followed by enantioselective HPLC AD-H of compound **5d**.

Once complete racemization was reached, the experimental values were collected and interpolated by a first order reversible kinetic equation and the rate constant ( $k_{TC}$ ) values referred to different temperatures were obtained.



$$\ln (x-x_{eq}) = (x_0-x_{eq}) - 2 k_{TC} t$$

x: molar fraction that is interconverting

$x_{eq}$ : molar fraction of the same enantiomer reached at the equilibrium state (0.5)

$x_0$ : initial molar fraction of the chosen enantiomer

$k_{Tc}$ : rate constant

t: time steps (s)

Function is the equation of a straight line  $y = mx + q$  with a slope of  $-2k_{Tc}$ , the intercept is  $\ln(x-x_{eq})$  and t is the independent variable of the function.

Then, the resulting  $k_{Tc}$  value, independent upon concentration, was used to derive the free energy of activation ( $\Delta G^\ddagger$ ) at each temperature by the Eyring equation,<sup>22</sup> where T is the absolute temperature.

$$k_{Tc} = \kappa \frac{k_B \cdot T}{h} e^{\frac{\Delta G^\ddagger}{RT}}$$

$h$  = Plank's constant ( $1.584 \cdot 10^{-34}$  cal·s)

$k_B$  = Boltzmann's constant ( $3.2998 \cdot 10^{-24}$  cal·K<sup>-1</sup>)

$R$  = universal gas constant ( $1.9872$  cal·K<sup>-1</sup>·mol<sup>-1</sup>)

$\kappa$  = transmission coefficient (1)

Explicating the  $\Delta G^\ddagger$  in kcal·mol<sup>-1</sup> we obtain:

$$\Delta G^\ddagger = 4.574 \cdot 10^{-3} \cdot T \cdot \left( \log \frac{T}{k_{Tc}} + 10.318 \right)$$

This is the value obtained experimentally with which we compare the theoretical results.

Table 6 shows the racemization trend at the temperature chosen for the kinetic studies of the compound **5d**. As we can see from the graphic and table, the experimental values follow a linear trend typical of the reversible first order kinetic.



Table 6. Compound **5d**: racemization process at each temperature of first eluted atropisomer.

T (°C)	T (s)	$\ln(x_0 - x_{eq})$	$x_{1 \cdot eluted}(\%)$	$x_{2 \cdot eluted}(\%)$
+50	0	-0.76852	96.37	4.63
	1800	-0.81193	94.4	5.60
	3720	-0.87155	91.83	8.17
	6420	-0.97206	87.83	12.17
	9120	-1.09512	83.45	16.55
+45	0	-0.78679	95.53	4.47
	3720	-0.84444	92.98	7.02
	7440	-0.91604	90.01	9.99
	10440	-0.97418	87.75	12.25
	15540	-1.07441	84.15	15.85
+40	0	-0,77936	95.87	4.13
	6840	-0,84513	92.95	7.05
	13260	-0,92332	89.72	10.28
	22080	-1,01888	86.10	13.90
	27840	-1,08560	83.77	16.23

Once obtained the  $k_{Tc}$  values we have calculated the energy of rotational barrier ( $\Delta G^\ddagger$ ) through the Eyring equation and the results are collected in Table 7.

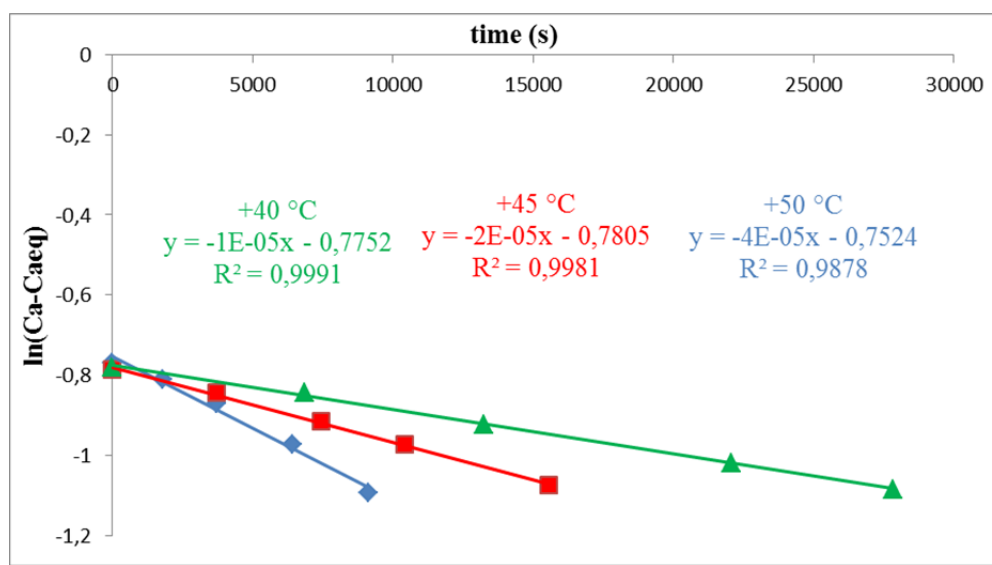


Figure 19. Kinetic data fitted with linear regression relative to thermal racemization of first eluted atropisomer.

Table 7. Rate constant and activation energies of interconversion of compound **5d**.

Compound <b>5d</b>	T = +40 °C	T = +45 °C	T = +50 °C
<b>k (s<sup>-1</sup>)</b>	$5.54 \cdot 10^{-6}$	$9.33 \cdot 10^{-6}$	$1.80 \cdot 10^{-5}$
<b><math>\Delta G^\ddagger</math> (kcal·mol<sup>-1</sup>)</b>	25.9	26.0	26.0

The energy values of the rotational barrier can be considered invariant with the temperature, taking into account the errors in the determination of the sample temperature. This implies a negligible  $\Delta S^\ddagger$ . Finally, the obtained experimental value of 26.0 kcal·mol<sup>-1</sup> is very well comparable with the theoretical values of 25.3 kcal·mol<sup>-1</sup> (Table 5). The half-life time was calculated applying the follow equation:

$$t_{\frac{1}{2}} = \frac{\ln 2}{k_{Tc}}$$

The resulting value is 30 days, so this product can be included into the 2b class of LaPlante.

#### 4. Absolute configuration of compound 5d

The absolute configuration was assigned to the two enantiomerically pure atropisomers of compound **5d** (the other compounds are too stereolabile to be able to assign it) using electronic circular dichroism (ECD) that is a technique become important in recent years thanks to the development of theoretical methods for the prediction of these properties based on the time-dependent density functional theory (TD-DFT).

The ECD spectra were acquired in the 190-400 nm region using a JASCO J-810 spectropolarimeter in HPLC-grade acetonitrile solution (Figure 20, bottom). Concentration was about  $1 \cdot 10^{-4}$  M, optimized in order to have a maximum absorbance between 0.8 and 1 (UV/vis in figure 20 up), with a cell path of 0.2 cm. The spectrum was obtained by the sum of 8 scans at  $50 \text{ nm} \cdot \text{min}^{-1}$  scan rate.

The ECD spectrum shows a large negative band at 235 nm and a positive one at 225 nm due to the naphthyl and to the 1,2-dibenzoazaborine chromophores.

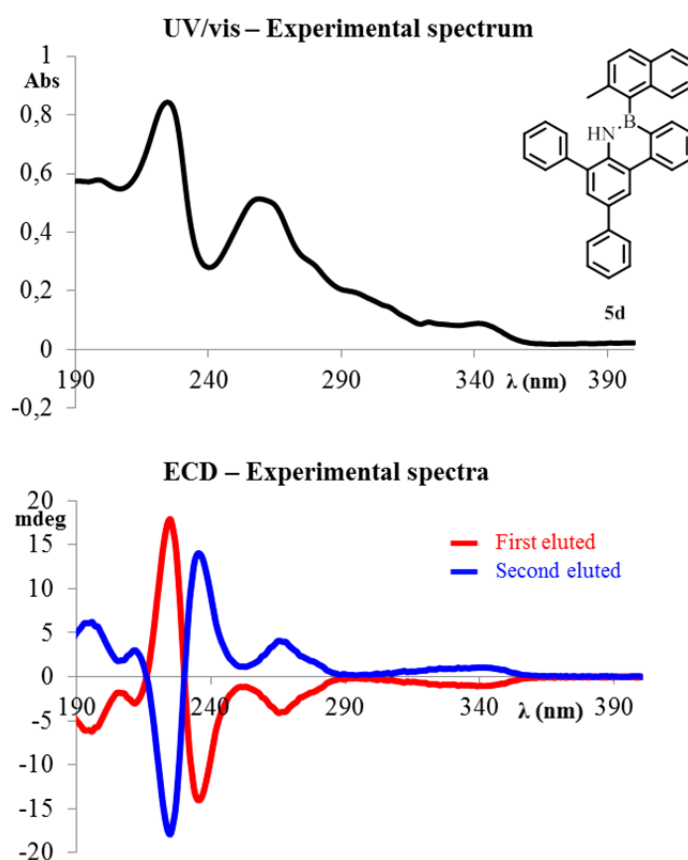


Figure 20. Up: experimental UV/Vis spectrum of compound **5d**. Bottom: experimental ECD spectra of first and second HPLC eluted **5d** (for the HPLC elution see figure 17).

The conformational research performed on all atropisomeric structures has shown that compound **5d** has four populated conformations which were used to calculate the ECD spectra. To compare the experimental results with theoretical ones, all calculated ECD spectra must be weighted by means of the Boltzmann equation.

The theoretical ECD spectra of all optimized ground state conformations (Figure 21) were obtained with various functionals to obtain a redundancy of the result and with a 6-311++g(2d,p) bases set. The most common ones are hybrid functional such as BH&HLYP,<sup>23</sup> M06-2X,<sup>24</sup>  $\omega$ B97XD<sup>25</sup> that includes empirical dispersion and CAM-B3LYP that includes long range correction using the Coulomb Attenuating Method.<sup>26</sup>

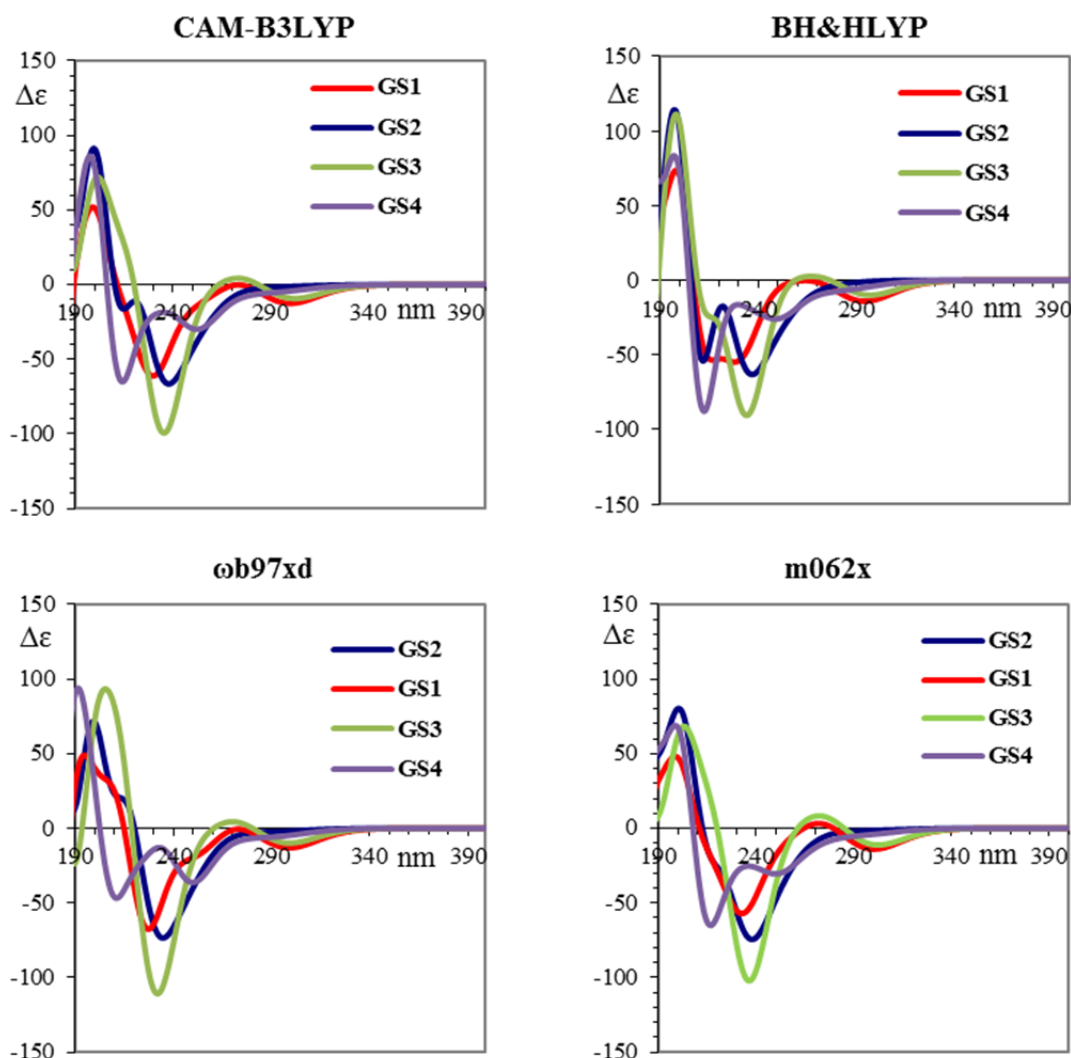


Figure 21. Computed spectra for the four stable ground states of *M* atropisomers of compound **5d**.

In each section of Figure 21 we can notice the four curves related to the four ground states for each functional. They are very similar with a negative band between 220 and 250 nm and one positive between 190 and 210 nm. For this reason, the final simulated spectrum, obtained by the weighted average of the four spectra, will not be sensitive to the conformational ratio at a great extent. In Figure 22, for each quadrant, the colored lines correspond to the weighted sum with Boltzmann distribution of the respective four simulated curves of Figure 21, obtained using the populations derived from B3LYP/6-31G(d,p) optimization, while the black line corresponds to the experimental spectrum of the first eluted atropisomer on Chiral Pak AD-H. The calculated spectra have been red shifting by 14, 16, 15 and 14 nm and multiplied by a factor 0.25, 0.19, 0.31, and 0.27 respectively for CAM-B3LYP, BH&HLYP,  $\omega$ B97XD and M06-2X.

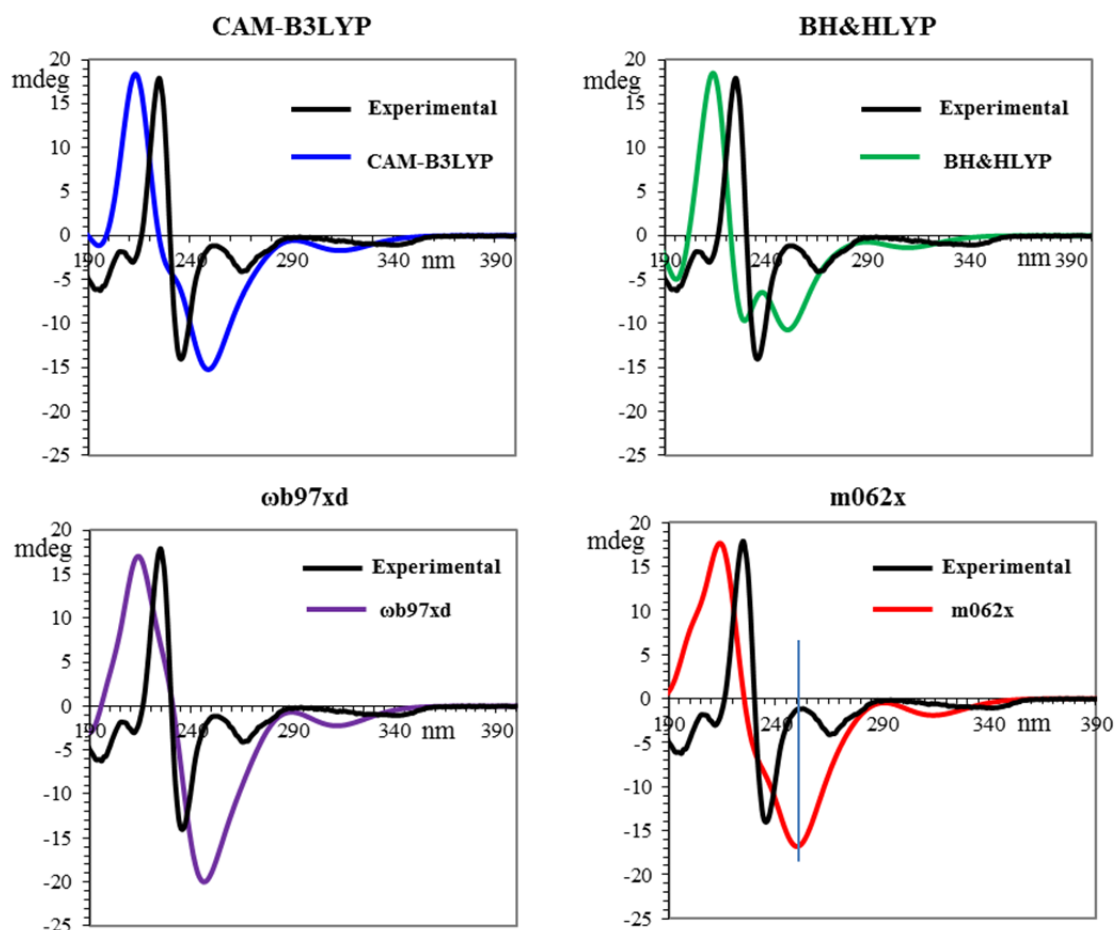


Figure 22. Experimental and calculated ECD of the first eluted atropisomers of **5d**.

The TD-DFT simulation for the *M* atropisomer fits very well with the experimental ECD spectrum of the first HPLC eluted **5d**. This convergence of the data is a good result of the whole stereochemical assignment, therefore the first eluted atropisomer has *M* configuration and the second one is the *P* atropisomer.

It should be noted that the GS4 calculated spectrum is the most similar to the experimental spectrum, so it appears that it is the most populated conformation in acetonitrile (Figure 23). This inconsistency could be due to the absence of the solvent in the optimization steps that were run in gas-phase conditions. However, when the optimization step was run including the solvent in the calculations<sup>27</sup> and at a higher level of theory (PCM method and 6-311G(2d,p) basis set), the results were very similar to that obtained in the gas-phase.

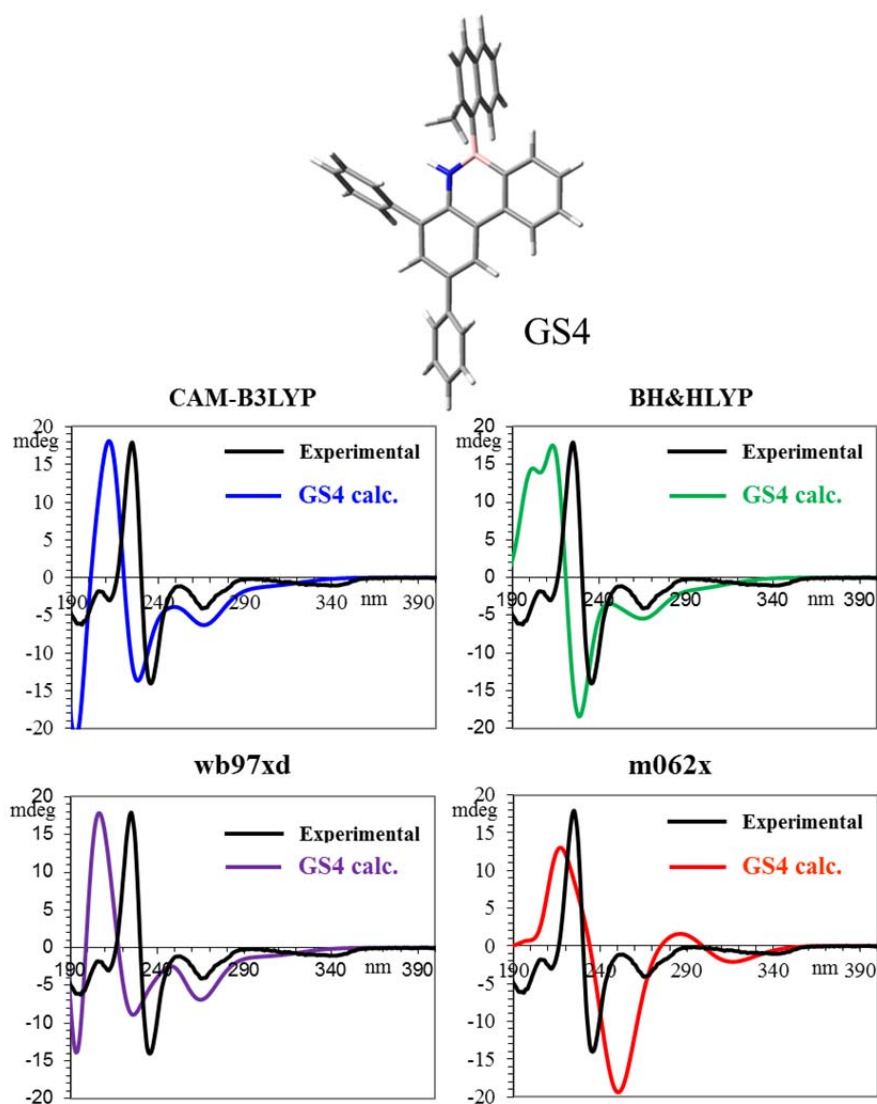


Figure 23. Experimental ECD of the first eluted atropisomer of **5d**, and calculated ECD spectrum, taking into account only the GS4 conformation.

## 5. Conclusion

We decided to focus our attention on the research of a new synthetic route for the preparation of atropisomeric 1,2-dibenzoazaborine bearing a stereogenic boron-aryl axis.

The synthetic procedure was optimized for compound **5a** with smallest steric hindrance and then we introduced a chirality probe in order to determinate the rotational energy barrier by dynamic NMR studies (i.e. ethyl in the product **5b** and isopropyl in the product **5c**). Moreover, the steric hindrance was increased to obtain a stable atropisomer **5d**.

Parallel to the optimization of the synthetic route, we have predicted the conformational stability by means of DFT calculations of ground and transition states.

Then we have analyzed the molecules with variable temperature NMR spectroscopy (**5b**), dynamic HPLC and racemization monitored by ECD (**5c**) and kinetics studies (**5d**) obtaining the energy barriers of 12.6, 21.8 and 26.0 kcal·mol<sup>-1</sup> for **5b**, **5c** and **5d** respectively (Table 8).

Table 8. Summary of results. Free energy values are reported in kcal·mol<sup>-1</sup>.

Compound	$\Delta G^{\#}_{\text{cal}}$	$\Delta G^{\#}_{\text{exp}}$	$t_{1/2}$	<u>LaPlante classification</u>
<b>5b</b>	13.2	12.6	0.19 ms	1
<b>5c</b>	21.5	21.8	18 min	2a
<b>5d</b>	25.3	26.0	15 days	2b

Once determined the interconversion energy barrier values of all the compounds, we have calculated the half-life time  $t_{1/2}$  at room temperature and from these results, we can affirm that compound **5b** belongs to the Class 1 of LaPlante classification scheme, while the compounds **5c** and **5d** belong to the Class 2a and 2b, respectively.

Finally, we have assigned the absolute configuration of the atropisomers for the compound **5d** by ECD (Electronic Circular Dichroism) methods and by TD-DFT.

The *M* absolute configuration was assigned to first eluted and the *P* absolute configuration to second one, on Chiral Pak AD-H columns.

In summary, we have found an accessible route synthesis in two steps without glove box obtaining good yields and a new atropisomeric compound that could have different optical properties respect to their all carbon form. The next step should be the introduction of a second chiral axis in order to obtain diastereomeric compounds.

## **6. Experimental section**

### **6.1 Materials**

The reagents used, commercially available, are as follows: 2,4,6-tribromoaniline, phenylboronic acid, bromoethyl, 2-ethylbromobenzene, iodoethane, 2-iodopropane, 1-bromo-2-naphthol,  $K_2CO_3$ , KHMDS, TMEDA/*n*-BuLi,  $Pd(PPh_3)_4$ , Mg (0),  $BCl_3$ , and  $AlCl_3$ . The solvents used are dry THF, dry toluene, dry  $Et_2O$ , DMSO and CPME.  $Et_2O$  and THF were dried prior to use by distillation with Na/benzophenone and toluene was distilled on  $CaH_2$  and stored anhydrous on molecular sieves. Deuterated solvents for NMR spectra are commercially available.

### **6.2 Instruments**

The stationary phase used for the chromatographic column is composed of 60 Å Silica gel (230-400 mesh, Sigma Aldrich) suitable for flash chromatography column. Silica gel plates 60 F254 (Merck) were used for the TLCs. Reactions requiring anhydrous conditions are made under nitrogen flow (inert atmosphere). The glassware used in these conditions was prepared by heating it to +70 °C at least three hours before the reaction. The Waters 600 HPLC with a wavelength set at 254 nm was used to purify the products. The columns used are described in the product characterizations. The  $^1H$ -NMR,  $^{13}C$ -NMR and  $^{11}B$ -NMR spectra were recorded with Varian Inova 600 MHz, Varian Mercury 400 MHz and Varian Gemini 300 MHz spectrometers. The chemical shifts are given in ppm relative to the internal tetramethylsilane standard ( $^1H$  and  $^{13}C$ ) or relative to the peak of the residual solvent. The assignment of the multiplicity of the carbons is obtained by means of the DEPT sequence. The low temperature spectra were conducted with an anhydrous nitrogen flow which cooled the coil at the base of the instrument. Inside the probe, on the other hand, a Cu/Ni thermocouple measures and regulates the temperature so that it remains fixed. The temperature calibration is done using a digital thermometer and the thermocouple. Then, a calibration line is needed

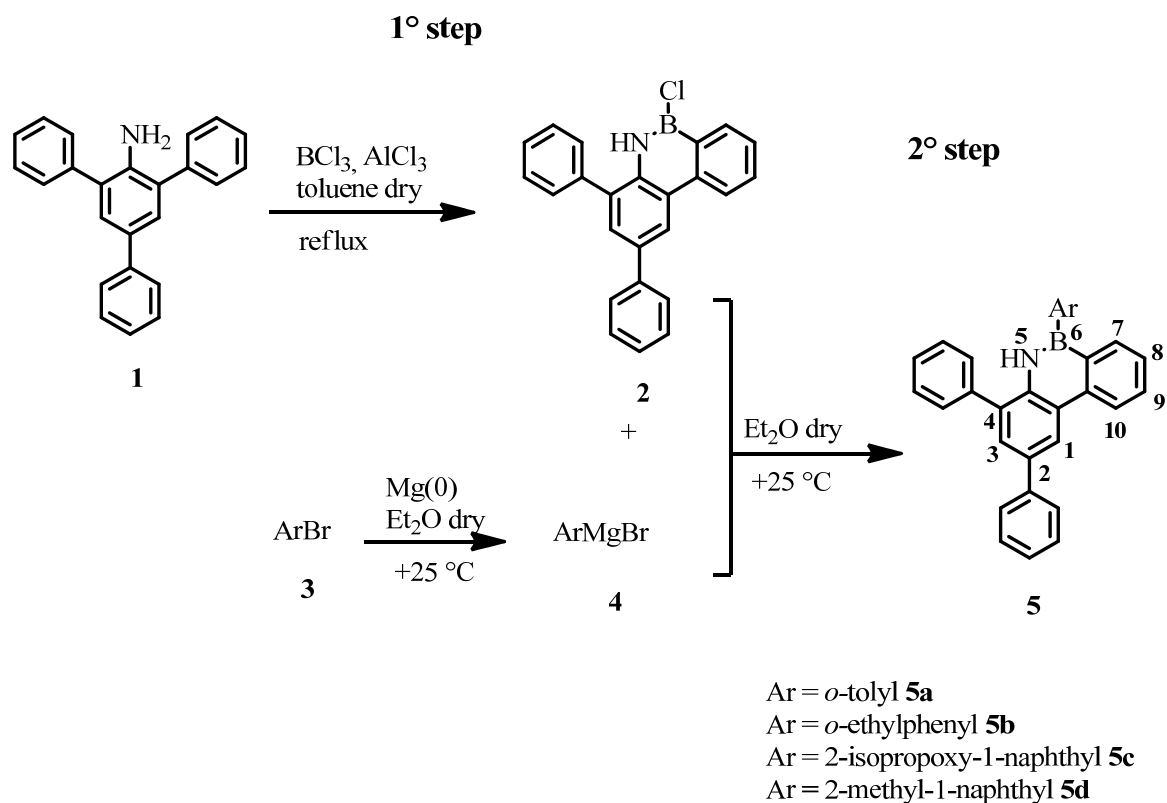
because the temperature is not measured throughout the probe. In fact, there will be variations with respect to the base, where I have the thermocouple and the upper part where there is placed. The measurement uncertainty can be estimated around  $\pm 1$  °C.

### 6.3 Computational calculations

A preliminary conformational research was performed using the molecular mechanics force field (MMFF), using the ComputeVOA 0.1 program. The most stable conformers found were subsequently minimized in energy with DFT computational calculations (Density Functional Theory), using Gaussian 16, rev. A.03, i.e. and the standard parameters of optimization. The B3LYP hybrid Functional and the 6-31G(d) basis set were used to calculate the ground states and the transition states. The analysis of the vibrational frequencies for each optimized structure showed the absence of imaginary harmonic frequencies for the fundamental states while for the transition states there is the presence of a single imaginary frequency. TD-DFT calculations were run using BH&HLYP, M06-2X,  $\omega$ B97XD, CAM-B3LYP and the 6-311++G(2d,p) basis set. 90 discrete transitions were calculated for each conformation (lowest calculated wavelength about 160 nm) and the ECD spectrum was obtained by convolution of Gaussian shaped lines (0.25 eV line widths). The simulated spectra resulting from the Boltzmann averaged sum of the conformations were vertically scaled and red-shifted by 14-16 nm to get the best simulations with the experimental spectra.

## 6.4 Synthesis and Characterization

The 1,2-dibenzoazaborine were synthesized following the synthetic schemes shown below.



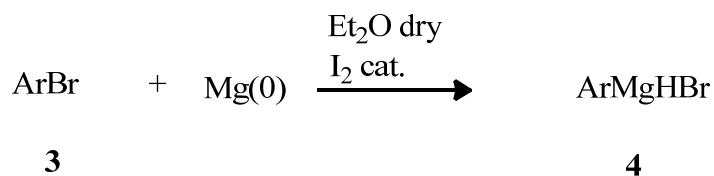
### 6.4.1 2,4,6-triphenyl-aniline 1

To a solution of compound **1** (2 g, 6.1 mmol) in 20 mL toluene/CPME 19:1 compound **2** (2 g, 20 mmol) and an aqueous solution of  $K_2CO_3$  (2 M, 15 mmol) were added. The mixture was degassed with vacuum/nitrogen cycles. A catalytic amount of  $Pd(PPh_3)_4$  is then added under nitrogen flow and then left to reflux for 24 hours. The ball was kept in the dark to avoid turning off the palladium. Finally, the reaction was quenched with water and the organic part was separated from the aqueous one, dried with  $Na_2SO_4$  and finally purified by a crystallization in hot acetonitrile. The product appeared as a white solid and it was obtained with good yields  $\approx 90\%$  (CAS: 6864-20-6).

**<sup>1</sup>H-NMR** (600 MHz, CD<sub>3</sub>CN, 1.96 ppm, +25 °C): δ 3.98 (bs, NH<sub>2</sub>), 7.28 (tt, J = 7.4, 1.1 Hz, 1H), 7.39-7.42 (m, 6H), 7.51 (tt, J = 7.3, 1.3 Hz, 4H), 7.57 (d, J = 1.1 Hz, 2H), 7.58 (t, J = 1.3, 2H), 7.61 (dd, J = 7.3, 2.0 Hz, 1H), 7.62 (t, J = 2.0 Hz, 1H).

**<sup>13</sup>C-NMR** (150.8 MHz, CD<sub>2</sub>Cl<sub>2</sub>, 53.52 ppm, +25 °C): δ 126.3 (CH), 126.4 (CH), 127.5 (CH), 128.3<sub>2</sub> (CH), 128.3<sub>4</sub> (Cq), 128.8 (CH), 129.0 (CH), 129.4 (CH), 130.8 (Cq), 139.8 (Cq), 139.8 (Cq), 140.6 (Cq), 140.9 (Cq).

#### 6.4.2 Aryl Grignard preparation **4**



0.75 g (30 mmol) of Mg (0) in 10 mL of dry Et<sub>2</sub>O was added to a two-necked flask equipped with a magnetic stir bar. These were left under stirring for one night. To this solution an iodine trowel tip was added as catalyst and reaction indicator. Finally, 1.26 mL (10 mmol) of aryl-bromide (**3**) was dropwise, which reacts by discolouring the solution from red to colourless. It is reacted for 1 hour obtaining a 0.5 M solution in Et<sub>2</sub>O.

#### 6.4.3 General procedure for the preparation of 1,2-dibenzoazaborinine **5**

The reaction was made following the Scheme 1. It was carried out in a two-necked flask under nitrogen atmosphere. The reflux condenser was fitted with a drying tube packed with calcium chloride. The trap was necessary because a large amount of hydrogen chloride develops, and this is corrosive for the tubes that connect the reaction flask to the nitrogen source. To a solution of product **1** (500 mg, 1.56 mmol) in dry toluene (20 mL), BCl<sub>3</sub> (4.7 mL, 1 M, 3 eq) was added dropwise at 0 °C. A precipitate has been formed when the BCl<sub>3</sub> solution was added, but it gradually dissolved, and the reaction

becomes clear again. Then the reaction was heating to reflux for 1/2 h under stirring and again it was cooled to room temperature. Thereafter, a catalytic amount of AlCl<sub>3</sub> was added to the suspension and the reaction is brought back to reflux and left under stirring for 18 hours. The product **2** was thus obtained. When the reaction was over, it was dried under vacuum, to remove the solvent, all traces of water and volatile components as hydrogen chloride and boron chloride. A green solid was obtained in which the dry Et<sub>2</sub>O (24 mL) is then redissolved. Finally, a Grignard solution **4** (4 mL, 0.5 M) freshly prepared in another two-necked flask and was added to the intermediate **2**. The resulting mixture was left under magnetic stirring for 1 hour. The reaction was quenched with water and filtered on a layer of silica gel and a layer of celite with EtOAc. Then, the organic layer was dried over of magnesium sulphate. The crude product **5** was so obtained. The product was purified with a chromatographic column (petroleum ether/EtOAc 9.5:0.5). Moreover, compounds **5a** and **5b** were purified by HPLC, with a Synergi 4u Polar – RP 80Å column. In all cases, the final product appears as a white solid. For each product the obtained yields were about of 31%.

#### 2,4-diphenyl-6-(*o*-tolyl)-5,6-dihydrodibenzo[*c,e*][1,2]azaborine **5a**

<sup>1</sup>H-NMR (600 MHz, CD<sub>2</sub>Cl<sub>2</sub>, 5.33 ppm, +25 °C): δ 2.20 (s, 3H), 7.10 (t, J = 7.4 Hz, 1H), 7.14 (d, J = 7.5 Hz, 1H), 7.19 (td, J = 7.6, 1.6 Hz, 1H), 7.26-7.31 (m, 2H), 7.34 (tdd J = 7.5, 1.8, 1.3 Hz, 1H), 7.37-7.50 (m, 5H), 7.46-7.50 (m, 2H), 7.59 (d, J = 2.1 Hz, 1H), 7.66-7.72 (m, 3H), 7.77 (dd J = 7.4, 1.2 Hz, 1H), 7.89 (bs, NH), 8.58 (d, J = 8.3 Hz, 1H), 8.66 (d, J = 2.1 Hz, 1H).

<sup>13</sup>C-NMR (150.8 MHz, CD<sub>2</sub>Cl<sub>2</sub>, 53.52 ppm, +25 °C): δ 22.6 (CH<sub>3</sub>), 121.8 (CH), 122.5 (CH), 123.9 (Cq), 124.7 (CH), 126.3 (CH), 127.0 (CH), 127.0 (CH), 128.1 (CH), 128.18 (CH), 128.3 (CH), 128.8 (CH), 129.3 (CH), 129.7 (CH), 131.2 (CH), 132.4 (Cq), 132.9 (CH), 134.1 (Cq), 135.3 (Cq), 136.5 (CH), 138.4 (Cq), 139.0 (Cq), 140.5 (Cq), 141.1 (Cq).

<sup>11</sup>B-NMR (192.4 MHz, CDCl<sub>3</sub>, BF<sub>3</sub>·Et<sub>2</sub>O, 0 ppm, +25 °C): δ 38.13.

HRMS(ESI-QTOF). Calcd. for C<sub>31</sub>H<sub>25</sub>BN<sup>+</sup> 422.2075. Found: 422.2071.

#### 6-(2-ethylphenyl)-2,4-diphenyl-5,6-dihydrodibenzo[*c,e*][1,2]azaborine **5b**

<sup>1</sup>H-NMR (600 MHz, CD<sub>2</sub>Cl<sub>2</sub>, 5.33 ppm, +25 °C): δ 1.05 (t, J = 7.6 Hz, 3H), 2.51 (q, J = 7.6 Hz, 2H), 7.11 (td, J = 7.2, 1.1 Hz, 1H), 7.19 (d, J = 7.6 Hz, 1H), 7.24 (td, J = 7.7, 1.2

Hz, 1H), 7.26-7.32 (m, 2H), 7.33-7.46 (m, 5H), 7.47-7.50 (m, 2H), 7.60 (d, J = 2.0 Hz, 1H), 7.68-7.72 (m, 2H), 7.74 (dd, J = 7.4, 0.9 Hz, 1H), 7.97 (bs, NH), 8.59 (d, J = 8.2 Hz, 1H), 8.67 (d, J = 1.9 Hz, 1H).

<sup>13</sup>C-NMR (150.8 MHz, CD<sub>2</sub>Cl<sub>2</sub>, 53.52 ppm, +25 °C): δ 16.4 (CH<sub>3</sub>), 29.6 (CH<sub>2</sub>), 121.9 (CH); 122.5 (CH), 124.1 (Cq), 124.9 (CH), 126.4 (CH), 127.1 (CH), 127.2 (CH), 127.8 (CH), 128.2 (CH), 128.4 (CH), 128.9 (CH), 129.4 (CH), 129.7 (CH), 131.3 (CH), 132.5 (Cq), 133.0 (CH), 134.2 (Cq), 135.4 (Cq), 136.7 (CH), 138.5 (Cq), 139.1 (Cq), 141.2 (Cq), 147.3 (Cq).

<sup>11</sup>B-NMR (192.4 MHz, CDCl<sub>3</sub>, BF<sub>3</sub>·Et<sub>2</sub>O, 0 ppm, +25 °C): δ 38.33.

HRMS(ESI-QTOF). Calcd. for C<sub>32</sub>H<sub>27</sub>BN<sup>+</sup> 436.2231. Found: 436.2233.

### 6-(7-isopropoxynaphthalen-1-yl)-2,4-diphenyl-5,6-dihydrodibenzo[c,e][1,2]azaborinine (**5c**)

<sup>1</sup>H-NMR (600 MHz, CD<sub>2</sub>Cl<sub>2</sub>, 5.33 ppm, +25 °C): δ 1.11<sub>6</sub> (d, J = 6.1 Hz, 3H), 1.12<sub>2</sub> (d, J = 6.1 Hz, 3H), 4.60 (sept, J = 6.1 Hz, 1H), 7.23 (qt, J = 6.8, 1.3 Hz, 1H), 7.30 (td, J = 6.8, 1.0 Hz, 1H), 7.35 (d, J = 9.1 Hz, 1H), 7.37-7.44 (m, 3H), 7.45-7.57 (m, 3H), 7.54 (t, J = 7.6 Hz, 2H), 7.62 (dd, J = 8.3, 1.2 Hz, 2H), 7.70 (dd, J = 6.9, 1.2 Hz, 1H), 7.74 (d, J = 1.9 Hz, 1H), 7.79-7.86 (m, 4H), 7.9 (d, J = 9.0 Hz, 1H), 8.29 (bs, NH), 8.74 (d, J = 8.3 Hz, 1H), 8.84 (d, J = 1.9 Hz, 1H).

<sup>13</sup>C-NMR (150.8 MHz, CDCl<sub>3</sub>, 77.36 ppm, +25 °C): δ 22.1 (CH<sub>3</sub>), 22.2 (CH<sub>3</sub>), 71.2 (CH), 116.4 (CH), 122.0 (CH), 122.5 (CH), 123.3 (CH), 124.2 (Cq), 125.7 (CH), 126.2 (CH), 127.1 (CH), 127.2 (CH), 128.0<sub>6</sub> (CH), 128.0<sub>9</sub> (CH), 128.4 (CH), 128.9 (CH), 129.2 (Cq), 129.3 (CH), 129.8 (CH), 130.1 (CH), 131.2 (CH), 132.4 (Cq), 135.8 (Cq), 136.8 (CH), 137.7 (Cq), 138.6 (Cq), 138.8 (Cq), 141.3 (Cq), 158.2 (Cq).

<sup>11</sup>B-NMR (192.4 MHz, CDCl<sub>3</sub>, BF<sub>3</sub>·Et<sub>2</sub>O, 0 ppm, +25 °C): δ 38.64.

HRMS(ESI-QTOF). Calcd. for C<sub>37</sub>H<sub>31</sub>BNO<sup>+</sup> 516.2493. Found: 516.2496.

### 6-(2-methylnaphthalen-1-yl)-2,4-diphenyl-5,6-dihydrodibenzo[c,e][1,2]azaborinine **5d**

<sup>1</sup>H-NMR (600 MHz, CD<sub>2</sub>Cl<sub>2</sub>, 5.33 ppm, +25 °C): δ 2.39 (s, 3H), 7.27 (qd, J = 6.8, 1.2 Hz, 1H), 7.36-7.46 (m, 5H), 7.46-7.54 (m, 3H), 7.56 (t, J = 7.5 Hz, 2H), 7.62 (dd, J = 8.3,

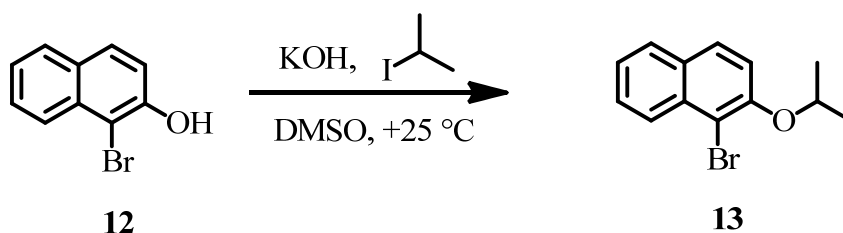
1.2 Hz, 2H), 7.65 (dd,  $J = 7.5, 1.3$  Hz, 1H), 7.76 (d,  $J = 2.0$  Hz, 1H), 7.82-7.88 (m, 5H), 7.27 (bs, NH), 8.77 (d,  $J = 8.3$  Hz, 1H), 8.87 (d,  $J = 1.7$  Hz, 1H).

$^{13}\text{C-NMR}$  (150.8 MHz,  $\text{CDCl}_3$ , 77.36 ppm, +25 °C):  $\delta$  22.9 ( $\text{CH}_3$ ), 122.1 (CH), 122.6 (CH), 124.4 (Cq), 124.6 (CH), 125.4 (CH), 126.6 (CH), 127.2<sub>0</sub> (CH), 127.2<sub>2</sub> (CH), 127.9 (CH), 128.1 (CH), 128.2 (CH), 128.5 (CH), 128.6 (CH), 128.8 (CH), 129.0 (CH), 129.4 (CH), 129.7 (CH), 131.5 (Cq), 131.6 (CH), 132.6 (Cq), 133.1 (bs, Cq), 134.4 (Cq), 135.6 (Cq), 136.6 (CH), 137.0 (bs, Cq), 138.4<sub>5</sub> (Cq), 138.4<sub>8</sub> (Cq), 139.0 (Cq), 141.2 (Cq).

$^{11}\text{B-NMR}$  (192.4 MHz,  $\text{CDCl}_3$ ,  $\text{BF}_3 \cdot \text{Et}_2\text{O}$ , 0 ppm, +25 °C):  $\delta$  39.40.

HRMS(ESI-QTOF). Calcd. for  $\text{C}_{37}\text{H}_{27}\text{BN}^+$  472.2231. Found: 472.2228.

#### 6.4.4 1-bromo-2-isopropoxynaphthalene (**9**)



In a flask 1-bromo-2-naphthol (**12**) (2.23 g, 10 mmol) was solubilized in the minimum amount of DMSO ( $\approx 20$  mL), to this an aqueous solution of KOH (3 mL, 4M, 12 mmol) was added. The reaction has been left under stirring at room temperature for about 15 minutes to allow the base to act. Once the ion has been formed, perceptible by a change of colour, the 2-iodopropane (2 mL, 20 mmol) was added. The reaction was left under mechanical stirring for two hours. Once the reaction is finished, the organic phase was separated by the aqueous phase, it is dried and finally, the solution was purified with a chromatographic column (petroleum ether/DCM, 9:1). The obtained yield was about 97%.

$^1\text{H-NMR}$  (600 MHz,  $\text{CDCl}_3$ , TMS, +25 °C):  $\delta$  1.36 (d,  $J = 6.1$  Hz, 6H), 4.59 (q,  $J = 6.1$  Hz, 1H), 7.14 (d,  $J = 8.9$  Hz, 1H), 7.33 (t,  $J = 7.5$  Hz, 1H), 7.50 (t,  $J = 7.6$  Hz, 1H), 7.67 (d,  $J = 8.9$  Hz, 1H), 7.70 (d,  $J = 8.3$  Hz, 1H), 8.21 (d,  $J = 8.5$  Hz, 1H).

**<sup>13</sup>C-NMR** (150.8 MHz, CDCl<sub>3</sub>, 77.36 ppm, +25 °C): δ 22.7 (2CH<sub>3</sub>), 73.6 (CH), 111.7 (Cq), 117.9 (CH), 124.7 (CH), 124.7 (CH), 126.7 (CH), 127.7 (CH), 128.2 (CH), 128.9 (CH), 130.4 (Cq), 133.6 (Cq), 152.9 (Cq).

## **7. Appendix**

### **7.1 Density Functional Theory DFT**

Computational studies performed with Density Functional Theory model (DFT) are nowadays widely used as theoretical support to experimental analysis which are made to determine the conformational stability of organic molecules. Conformational calculation of organic molecules was mainly performed by molecular mechanics and semi-empirical methods. DFT method, proposed by Kohn and Sham, is one of them, DFT predicts a great variety of molecular properties: molecular structures, vibrational frequencies, atomization energies, ionization energies, electric and magnetic properties, reaction paths, etc.<sup>28</sup> Density functional theory (DFT) is the most popular and versatile computational quantum mechanical modelling method used in physics, chemistry and materials science to investigate the electronic structure (principally the ground state) of many-body systems, in particular atoms, molecules, and the condensed phases.<sup>29</sup> DFT method also determines the properties of a many-electron system using functional, which allow us to see the electronic density of the considered molecules.

The functionals normally used in DFT are integrals of function of density and eventually its gradient. In the '90 Functional B3LYP becomes popular. This type of functionals linearly combines the Hartree-Fock exchange with DFT exchange-correlation functionals, leading to integrals that can be solved only by numerical methods, but having a much wider application especially in the field of organic chemistry. The Hartree-Fock (HF) method is a method of approximation for the determination of the wave function and the energy of a quantum many-body system in a stationary state.<sup>29</sup> The others method used are MM3, MMX, MMFF, etc. In contrast to DTF, these methods have intrinsic limitation. Usually the rotational energy barriers were calculated by moving the relative part of the molecule in fixed steps and optimizing the remaining part. The transition states were assumed "handmade" and the geometry was optimized within certain constraints. So, in the other methods there were a lot of approximation and the result were obtained with a large error, and there was no guaranteed that a real transition state had been located.<sup>30</sup> Moreover, acceptable results could be obtained only with small

molecular structures. Instead, DTF method has the great advantage of taking account of electronic correlation at a reasonable computational cost.<sup>31</sup> Density functional Method is based on the idea that for a collection of nuclei and electrons the ground state molecular energy, the wave-function and all other molecular electronic properties are uniquely determined by the electron probability density  $\rho(x,y,z)$ , a functional of three variables. The ground state energy,  $E_0$ , is a functional of  $\rho$ :  $E_0 = F[\rho]$ .<sup>32</sup> Recently, the development of highly persuasive servers allowed high-level calculations to be performed in an amount of acceptable time for even large enough molecules, 50-60 atoms. DFT can be used both to obtain the conformation of ground states and also to find the correct geometries and energies of transition states. The very interesting thing is that thanks to vibrational analysis, there is always confirmation that the correct transition state has been unambiguously identified.

### Ground state (GS)

In recent years, in literature, many papers addressing the performance of various DFT functionals in determining relative energies in reaction have appeared,<sup>33</sup> but for conformational analysis there have been very few. The smallest basis set used is generally 6-31G(d) or the equivalent. Basis set in theoretical and computational chemistry is a set of functions (called basis functions) that is used to represent the electronic wave function.<sup>29</sup> Due to the fact that the density functional has limited accuracy compared to the basis set, there is only a small increase in accuracy obtained by using very large basis set. So, the accuracy of results from DFT calculations depends on the choice of the basis set and density functional. The relative energies of conformations can be compared with the results of kinetic studies. DFT studies compare very well with experimental observation in almost all cases, and the relative energies of possible conformations are correctly calculated. The computational of vibrational frequency verifies if in a ground state is not shown the presence of any imaginary harmonic frequencies.

### Transition states (TS)

The determination of transition state energy and structure is very important to the stereodynamic analysis. In fact, it represents the energy barrier involved into the

interconversion process between the two atropisomers. D. Young defined the transition state as: *“the geometry that has zero derivative of energy with respect to moving every one of the nuclei, and has positive second derivative energy for all but one geometric movement”*<sup>34</sup>. This means that the transition states links two ground states, and represent a maximum of energy in the diagram, but is a minimum for all the other movement. On the contrary to ground state, the computational of vibrational frequency for the transition states shows the presence of a single imaginary frequency.

Unfortunately, in contrast with the transition states for high-energy processes (such as those involved in a chemical reaction), in which the imaginary frequency usually has a large and negative value, the transition states involved in internal dynamic processes usually display small negative vibrational frequencies and can therefore be difficult to locate, especially in the presence of other possible internal motions. On the other hand, the geometry of a transition state is much simpler to idealise, because many geometrical parameters are fixed by the molecular scaffold. The use of DFT in the study of conformational isomers and the ability to identify easily the transition state, allow to analyze the rotation energy barrier and to compare to the experimental one obtained with D-NMR (dynamic NMR), D-HPLC (dynamic HPLC) and kinetic studies.

## 7.2 Dynamic stereochemistry analysis and methodologies

Dynamic Nuclear Magnetic Resonance (D-NMR) and Dynamic High-Performance Liquid Chromatography (D-HPLC) are the most useful experimental methods to determine the conformational stability of organic molecules and the proprieties of such compound.

### 7.2.1 Dynamic Nuclear Magnetic Resonance D-NMR

The possibility that magnetic resonance might be used to measure chemical exchange rates was suggested explicitly by Gutowsky and Saika in 1953 and it was reduced to

practice in 1956 by Arnold, Gutowsky and Holm. Thirty years ago, Time-Dependent perturbation theory certainly was well understood.<sup>35</sup>

NMR is able to observe the conformational exchange of chemical species that happens at a rate sufficiently low to observe separate anisochronous signals, in the milliseconds-seconds region:

$$t = \frac{\sqrt{2}}{2\pi \Delta\nu}$$

where:

$t$  = conformational exchange time (s);

$\Delta\nu$  = chemical shift difference (in Hz) without exchange.

Through this equation we can see that two exchanging nuclei display different chemical shifts if they occupy two different positions in different magnetic environment for a longer time compared to the time of interconversion from one conformation to another. To analyze organic compound by Dynamic NMR, the time of kinetic process must be compatible with the time scale of the NMR acquisition. Analysis consists in the acquisition of spectra at different temperature. In this way, in each spectrum we can observe a different line shape, and this is the results of the conformational process taking place within the NMR time scale.

For example, if we have a chiral probe, when the rotation around the chiral axis is slow in the NMR time scale, we can see two different signals for the two CH<sub>3</sub> because the two hydrogen experiences a magnetically different environmental for a time long enough. If the rotation is fast in the NMR time scale, the two CH<sub>3</sub> give only one signal. Therefore, as the temperature changes we can obtain the two situations described and the intermediate situation defined as coalescence of the two peaks like is described in Figure 22.

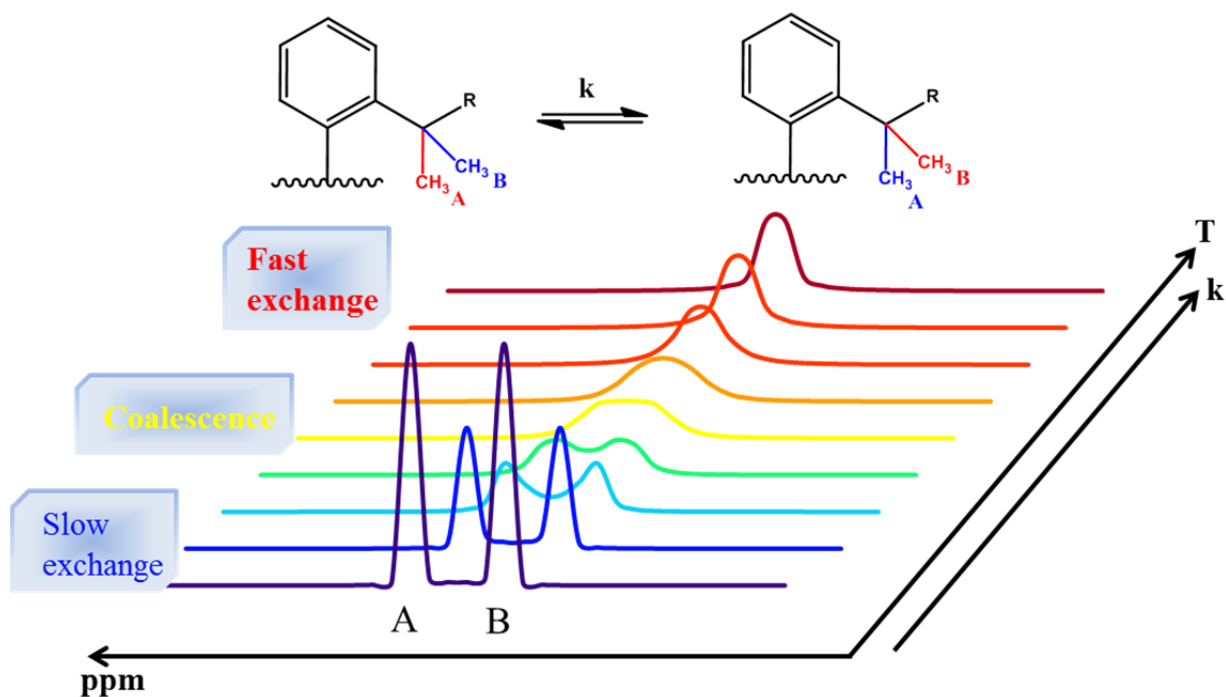


Figure 22. D-NMR profile of two CH<sub>3</sub> enantiotopic signal in chiral environment.

The rate constant interconversion can be calculated as

$$k_{Tc} = \pi \frac{\Delta\nu}{\sqrt{2}}$$

Where  $k_{Tc}$  is the rate constant at the coalescence temperature  $Tc$  and  $\Delta\nu$  is the chemical shift difference (Hz) without exchange (at low temperature). As you can see, it is a first order kinetics. However there are cases more complicated where the species shows different thermodynamic stability and more complicated NMR spectrum with several coupling constants.<sup>36</sup> In these cases,  $k_{Tc}$  is obtained by *line shape simulation* analysis of the Dynamic-NMR spectra through mathematical models that can simulate second-order spectra and quiet complex system.<sup>37</sup> This method consists in: a first simulated spectrum obtained where the dynamic process are frozen ( $k \approx 0$ ), then it simulates the line shape at higher temperature by changing the values of the rate constant. The D-NMR method can determine energy values between 4.5 and 21 kcal·mol<sup>-1</sup> by shape simulation. If the rotational energy barrier ( $\Delta G^\ddagger$ ) is bigger than 21-23 kcal·mol<sup>-1</sup>, it is not accessible with

this technique but, for the kinetic studies we can apply the Dynamic High-Performance Liquid Chromatography (D-HPLC).

### 7.2.2 Dynamic High Pressure Liquid Chromatography D-HPLC

Liquid-phase enantioseparation techniques are fruitfully applied in the separation of atropisomers when their qualitative and quantitative identification is requested.<sup>38</sup>

Molecules possess rapid interconversion can produce serious complications in drug development, as atropisomers can display drastically different pharmacological profiles.<sup>39</sup> To analyze rotational energy barrier ( $\Delta G^\ddagger$ ) in the range of 21-23 kcal·mol<sup>-1</sup>, D-HPLC can be used. When the two peaks on the spectrum are well separated by the base line, it means that the enantiomers separation was successful. If the chromatographic run is made at a temperature at which the two conformers interconvert, a plateau is observed between the two peaks. The interconversion rate and consequently the height of the plateau increase with increasing temperature until the complete coalescence of the peak occurs. D-HPLC is complementary to the D-NMR because enantiomers or atropisomer that interconvert can be analyzed without the presence of a *probe* of chirality. There more D-HPLC has a number of important advantages, such as low quantity of material needed for measurements, employment of non-deuterated solvents, and the possibility of physical isolation of isomers for further characterizations. Like to the D-NMR, the direct kinetic analysis can be performed by computer simulation of characteristic elution profiles that result from concurrent separation and interconversion of enantiomers on the column.<sup>40</sup> Simulation of the experimentally obtained elution profiles is a versatile tool to determine the rate constant of the observed on-column isomerization by an iterative optimization procedure that is completed when the calculated and the experimental elution profiles are superimposable.

### 7.3 Time Depend-Density Functional Theory TD-DFT

TD-DFT is an extension of density functional theory (DFT), and the conceptual and computational foundations are analogous. It is a quantum mechanical theory used in physics and chemistry to investigate the properties and dynamics of many-body systems in the presence of time-dependent potentials, such as electric or magnetic fields.<sup>41</sup>

### 7.4 Electronic Circular Dichroism ECD

One method used to detect and analyse chirality is the determination of the optical activity by electronic circular dichroism (CD).<sup>42</sup>

When a molecule contains one or more chiral chromophores we can see a difference in the absorption of left-handed circularly polarized light (L-CPL) and right-handed circularly polarized light (R-CPL). It is used to study structural, kinetic and thermodynamic information about chiral molecules of all types and sizes. Circular dichroism spectra are measured using a circular dichroism spectrometer. These types of spectrometers measure alternately the absorption of L- and R-CPL, usually at a frequency of 50 kHz, and then calculate the circular dichroism signal. According to the direction of the polarized light, therefore, it is possible to assign the absolute configuration to the enantiomers considered. Assigning the absolute configuration, as was also mentioned in the introductory part of the thesis is especially important in the biological field because two enantiomeric molecules can have different effects with the environment in which they interact and often, only one of them has positive effect, while another could be harmful. The first concept of polarized light is that of linear polarization, that is a wave that oscillates on a single plane which can be vertical or horizontal as show in the following Figure 23.

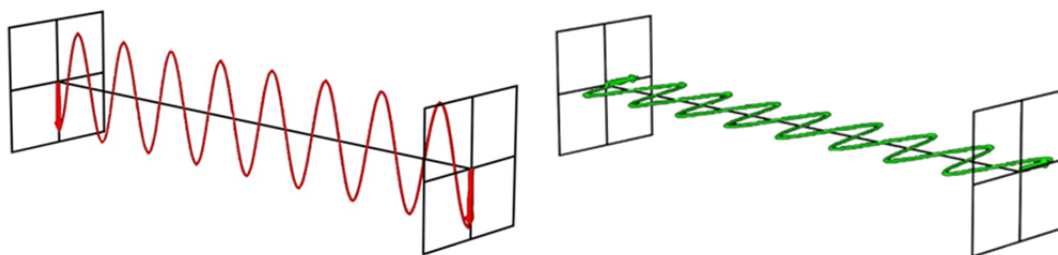


Figure 23. Vertically and horizontally Polarized Light.

If for instance we take horizontally and vertically polarised light waves of equal amplitude that are in phase with each other, the resultant light wave is linearly polarised at 45 degrees (Figure 24).

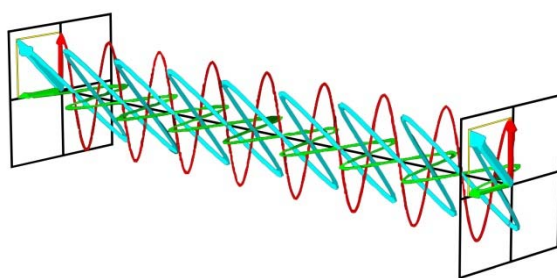


Figure 24. 45° Polarized Light.

If the two first linear polarized waves are out of phase, the resulting wave was not linearly polarized, but the resultant will be a helix and it is known as circularly polarized light (CPL). The helices can be either right-handed (R-CPL) or left-handed (L-CPL) and are non-superimposable mirror images. In the instrument used, a suitably oriented plate will convert linearly polarized light into circularly polarized light by slowing one of the linear components of the beam with respect to the other so that they are one quarter-wave out of phase. This will produce a beam of either left- or right-CPL.

The difference in absorbance of left-hand and right-hand circularly polarized light is the basis of circular dichroism. A compound that absorbs L-CP or R-CP, is optically active, or chiral (Figure 25).

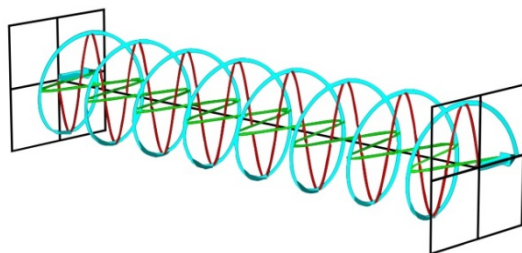


Figure 25. Left Circularly Polarized Light (LCP).

Chiral molecules exhibit circular birefringence, which means that a solution of a chiral substance, through which left circularly polarized light or right circularly polarized light are propagate at different speeds. On traversing the circularly birefringent medium, the phase relationship between the circularly polarized changes and the resultant linearly polarized wave rotates. This is the origin of the phenomenon known as optical rotation. Circular dichroism (CD) is the difference in the absorption of left-handed circularly polarized light (L-CPL) and right-handed circularly polarized light (R-CPL) and occurs when a molecule contains one or more chiral chromophores (light-absorbing groups).

Circular dichroism is therefore given by the follow equation:

$$\Delta A(\lambda) = A(\lambda)_{L-CPL} - A(\lambda)_{R-CPL}$$

Where  $\lambda$  is the wavelength.

CD may be regarded as one of the most powerful techniques for stereochemical analyses: it is sensitive to the absolute configuration as well as to conformational features, which are often completely obscured in the ordinary absorption spectrum. A circular dichroism signal can be positive or negative, depending on whether L-CPL is absorbed to a greater extent than R-CPL (positive CD signal) or to a lesser extent (negative CD signal). The CD of pure enantiomers differs in sign, but not in magnitude and there isn't simple relation between the absolute configuration of an enantiomer and the sign of its ECD spectrum. In fact, CD depends on details of the electronic and geometric molecular structure.<sup>42</sup> For two enantiomers, one spectrum will be positive and the other negative. Furthermore, these will be specular to each other if the concentrations of the two solutions are identical.

## 8. References

---

- <sup>1</sup> Bosdet, M. J. D.; Jaska, C. A.; Piers, W. E.; Sorensen, T. S.; Parvez, M. *Org. Lett.* **2007**, *9*, 1395.
- <sup>2</sup> Wang, X.-Y.; Lin, H. R.; Lei, T.; Yang, D.-C.; Zhuang, F. D.; Wang, J. Y.; Yuan, S. C.; J. Pei *Angew. Chem. Int. Ed.* **2013**, *52*, 3117.
- <sup>3</sup> Mazzanti, A.; Mercanti, E.; Mancinelli, M. *Org. Lett.* **2016**, *18*, 2692–2695.
- <sup>4</sup> Smith, M. B., *March's Advanced Organic Chemistry: Reactions, Mechanisms, and Structure*, 7<sup>th</sup> edition, Cram 101, **2013**.
- <sup>5</sup> Pasteur, L. *Ann. Chim. Physique* **1848**, *24*, 442-459.
- <sup>6</sup> Reist, M.; Carrupt, P.A.; Francotte, E.; Testa, B. *Chem. Res. Toxicol.* **1998**, *11*, 1521-1528.
- <sup>7</sup> a) Ho, T.L. *Stereoselectivity in Synthesis*, Wiley-VCH, New York, **1999**; b) Lin, G.-Q.; Li, Y.-M.; Chan A.S.C. *Principles and Applications of Asymmetric Synthesis*, Wiley-VCH, New York, **2001**.
- <sup>8</sup> Oki, M. *Top. Stereochem.* **1984**, *14*, 1–81.
- <sup>9</sup> Laplante, S.P.; Edwards, P. J.; Fader, L.D.; Jakalian, A.; Hucke, O. *ChemMedChem*, **2011**, *6*, 503-513.
- <sup>10</sup> Fingerle, M.; Maichle-Mössmer, C.; Schundelmeier, S.; Speiser, B.; Bettinger, H.F. *Org. Lett.*, **2017**, *19* (17), 4428-4431.
- <sup>11</sup> Dewar, M.J.S.; Kubba, V. P. Pettit R. *J. Chem. Soc.* **1958**, *0*, 3073–3076.
- <sup>12</sup> <https://www.sciencedaily.com/releases/2010/10/101006085720.htm>
- <sup>13</sup> Maluenda, I.; Navarro, O.; *Molecules* **2015**, *20*, 7528-7557.
- <sup>14</sup> Molander, G. A.; Gormisky, P. E.; Sandrock D.L. *J. Org. Chem.*, **2008**, *73*, 2052-2057.
- <sup>15</sup> Dewar M.J.S.; Dietz, R.J. *Chem. Soc.* **1959**, 2728.
- <sup>16</sup> Dewar, M.J.S.; Dietz, R. *J. Chem. Soc.*, **1959**, *0*, 2728-2730.
- <sup>17</sup> Ishibashi, J.S.A.; Dargelos, A; Darring C.; Crhostowska, A; Liu, S.-Y. *Organometallic* **2017**, *36*, 2494-2497.
- <sup>18</sup> Jung, M.; Schurig, V. *J. Am. Chem. Soc.* **1992**, *114*, 529-534.
- <sup>19</sup> Pirkle, W.H.; Schreiner, J.L. *J. Org. Chem.* **1981**, *46*, 4988-4991.
- <sup>20</sup> a) Cirilli, R.; Costi, R.; Di Santo, R.; La Torre, F.; Pierini, M.; Siani, G. *Anal. Chem.*, **2009**, *81*, 3560; b) Veciana, J., Crespo, M.I. *Angew. Chem. Int. Ed.* **1991**, *30*, 74-77; c) Krupcik J.; Oswald, P.; Majek, P.; Sandra, P.; Armstrong, D.W. *J. Chromatogr. A* **2003**, *1000*, 779-800.
- <sup>21</sup> Lunazzi, L.; Mancinelli, M.; Mazzanti, A.; Lepri S.; Ruzziconi R.; Schlosser, M. *Org. Biomol. Chem.*, **2012**, *10*, 1847-1855.
- <sup>22</sup> Eyring, H. *Chem. Revs.* **1935**, *17*, 65-77.

- 
- <sup>23</sup> In Gaussian 09 the BH&HLYP functional has the form:  $0.5 * E_X^{HF} + 0.5 * E_X^{LSDA} + 0.5 * \Delta E_X^{Becke88} + E_C^{LYP}$
- <sup>24</sup> Zhao, Y.; Truhlar, D. G. *Theor. Chem. Acc.* **2008**, *120*, 215-241.
- <sup>25</sup> Chai, J. D.; Head-Gordon M. *Phys.Chem.Phys.* **2008**, *10*, 6615-6620.
- <sup>26</sup> Yanai, T.; Tewand, D.; Handy, N. *Chem. Phys. Lett.* **2004**, *393*, 51-57.
- <sup>27</sup> Tomasi, J.; Mennucci, B.; Cammi, R. *Chem. Rev.* **2005**, *105*, 2999-3094.
- <sup>28</sup> Cuevas, J. C. *Introduction to Density Functional Theory*, 2003, *14*, 29.
- <sup>29</sup> Brachrach, S. M., *Computational Organic Chemistry*, 2<sup>nd</sup> ed., **2014**.
- <sup>30</sup> Casarini, D; Lunazzi, L; Mazzanti A. *Eur. J. Org. Chem.* **2010**, *11*, 2035-2056.
- <sup>31</sup> Koch, M.; Holthausen, M.C.A. *Chemist's Guide to Density Functional Theory*, Wiley-VCH, Weinheim, 2<sup>nd</sup> ed., **2002**; *A Primer in Density Functional Theory* (EDs.: Fiolhais, C.; Nogueira, F.; Marques, M.), Springer-Verlag, Heidelberg, **2003**.
- <sup>32</sup> Mitchell, P.C.H. *Appl. Organometal. Chem.* **2000**, *14*, 744-747 in the preface to: *A Chemist's Guide to Density Functional Theory* Koch, W.; Holthausen, M. C. Wiley-VCH, Weinheim, 2<sup>nd</sup> ed., **2002**.
- <sup>33</sup> Check, C.E.; Gilbert, T. M. *J.Org.Chem.* **2005**, *70*, 9828- 9834; b) Wodrich, M. D.; Corminbouef, C.; Schleyer, P. v. R. *Org. Lett.* **2006**, *8*, 3631-3634; c) Shreiner, P. R.; Fokin, A. A.; Pascal, R. A.; De Mejere, A. *Org. Lett.* **2006**, *8*, 3635-3638; d) Grimme, S. *Angew. Chem. Int. Ed.* **2006**, *45*, 4460-4464; e) Zhao, Y.; Truhlar, D. G. *Org. Lett.* **2006**, *8*, 5753-5755; f) Rokob, T. A.; Hamza, A.; Pápai, I. *Org. Lett.* **2007**, *9*, 4279-4282; g) Shreiner, P. R. *Angew. Chem. Int. Ed.* **2007**, *46*, 4217-4219; h) Wodrich, M. D.; Wannere, C.S.; Mo, Y.; Jarowski, P.D.; Houk, K. N.; Schleyer, P. v. R. *Chem. Eur. J.* **2007**, *13*, 7731-7744; i) Zhao, Y.; Truhlar, D.G. *Acc. Chem. Res.* **2008**, *41*, 157-167; j) Schwabe, T.; Grimme, S. *Acc. Chem. Res.* **2008**, *41*, 569-579; k) Wodrich, M.D.; Jana, D.F.; Schleyer, P. v. R.; Corminbouef, C. J. *Phys. Chem.* **2008**, *112*, 11495-11500.
- <sup>34</sup> Young, D. *Computational Chemistry*, Wiley Interscience, New York, **2001**, chapter 17, pp. 147-158.
- <sup>35</sup> Sandström, J. *Dynamic NMR Spectroscopy*, Accademic Press. **1982**.
- <sup>36</sup> Toyota, S.; Makino, T. *Tetrahedron Lett.* **2003**, *44*, 7775-7778.
- <sup>37</sup> Brown, J.H.; Bushweller, C. H.; Mastergabin, J.C. QCPE Program No. 633, **1993**.
- <sup>38</sup> Peluso, P.; Mamane, V.; Aubert, E.; Cossu, S.; *Electrophoresis* **2017**, *38*, 1830-1850.
- <sup>39</sup> Smith, D.E.; Marquez, I.; Lokensgard, M.E.; Rheingold, A.L.; Hecht, D.A.; Gustafson, J. L., *Angew. Chem. Int.Ed.* **2015**, *54*, 11754-11759.
- <sup>40</sup> Trapp, O.; in Schurig, V. (Ed.), *Differentiation of Enantiomers II*, *Topics in Current Chemistry Series*. Springer International Publishing, Switzerland **2013**, 1231-269.
- <sup>41</sup> Marques, M.A.L.; Gross, E.K.U. *Annu. Rev. Phys.Chem.* **2004**, *55*, 427-455.
- <sup>42</sup> Warnke, I.; Furche, F. *WIREs Comput Mol Sci.* **2012**, *2*, 150-166.